

Dynamic Redeployment of Nurses Across Hospitals: A Sample Robust Optimization Approach

Wei Liu

Faculty of Business in Scitech, School of Management, University of Science and Technology of China, liuweimn@ustc.edu.cn

Tianchun Li

Elmore Family School of Electrical and Computer Engineering, Purdue University, li2657@purdue.edu

Mengshi Lu

Mitchell E. Daniels, Jr. School of Business, Purdue University, mengshilu@purdue.edu

Pengyi Shi

Mitchell E. Daniels, Jr. School of Business, Purdue University, shi178@purdue.edu

Problem definition: We study a workforce redeployment problem in hospital networks, where clinical staff, such as nurses, are temporarily reassigned from overstaffed to understaffed sites to address short-term imbalances. This practice of “internal travel,” which gained traction during the COVID-19 pandemic to tackle nurse shortages, presents new operational challenges that require tailored analytical support. Key requirements such as advance notice and short-term secondments must be incorporated. Moreover, in rapidly evolving environments, reliance on historical data leads to unreliable forecasts, limiting the effectiveness of traditional sample-based methods. **Methodology:** We formulate the problem as a stochastic dynamic program and incorporate demand uncertainty via a sample robust optimization (SRO) framework. Using linear decision rule approximation, we reformulate the problem as a tractable linear program. **Results:** We evaluate the impact of key network design components on system performance. Network connectivity has the largest effect in reducing the total cost, number of redeployments, and travel distance, but its benefits depend on aligning the secondment duration with the network structure. Full connectivity without proper secondments can be counterproductive. The SRO approach outperforms the traditional sample-average method in the presence of demand surges or under-forecasts by better anticipating emergency redeployments. **Managerial implications:** Internal travel programs offer a promising strategy to alleviate workforce shortages in healthcare systems. Our results highlight the importance of network design, aligning secondment durations with the network structure, and adopting planning methods that are robust to demand surges or inaccurate predictions.

Key words: workforce management, robust nurse staffing, inter-hospital transfer

1. Introduction

The decades-long healthcare workforce shortage has escalated into a global crisis, with the United States projected to face significant deficits across multiple frontline roles—including nurses, nurse assistants, and clinical technicians—by 2030 (Lyons 2023, Hoover et al. 2024 and Murphy 2024). These shortages have serious implications, including increased staff burnout, higher risks of medical errors, and adverse patient outcomes (University of St. Augustine for Health Sciences 2024,

Carayon and Gurses 2018). In response, a growing number of hospital systems have adopted “internal travel” programs, which temporarily redeploy medical staff across hospital sites to manage demand imbalances (Brenner 2025, and Yuan 2025). This practice, which emerged during the COVID-19 pandemic, introduces new operational challenges that demand tailored analytical support. Our community partner, Indiana University Health (IU Health), is one such system that has implemented the workforce redeployment initiative, termed the Delta Coverage program (Helm et al. 2024). Motivated by this context, our research in this paper focuses on nurse redeployment as a representative case, with the problem setup applicable to other roles such as nurse assistants and technicians. Next, we introduce the background and outline the key analytical challenges using IU Health as a motivating example, while highlighting the relevance in the broader healthcare context. We then present an overview of our approach and key contributions.

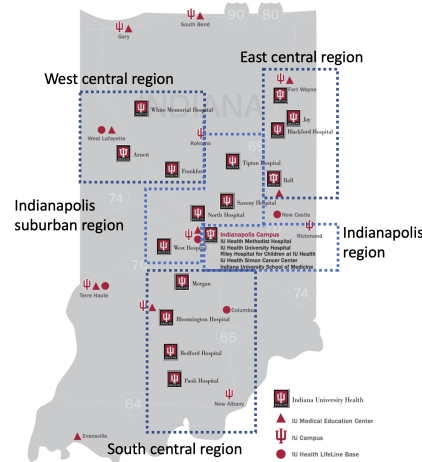


Figure 1 Locations of each hospital in the IU Health network.

1.1. Problem Background and Operations Challenges

IU Health is the largest healthcare system in Indiana, operating 16 hospitals. Figure 1 shows the distribution of these hospitals throughout the state, with four main regions segregated based on their proximity to Indianapolis (IU Health 2023). The central regions, including Indianapolis and its suburban areas, have higher population densities. During the early stages of the COVID-19 pandemic, they experienced more confirmed cases and hospitalizations (per 10,000 residents, Indiana State Government 2023), and hence, faced severe nurse shortages at the onset of the outbreak. In contrast, rural regions with lower population densities initially saw fewer cases but faced their unique challenges. With smaller staffing pools and limited surge capacity, these hospitals struggled to absorb day-to-day demand fluctuations. When COVID-19 eventually spread to these areas, they

experienced even more severe staffing shortfalls than their urban counterparts. This stochastic and regionally asynchronous demand pattern was a key driver behind IU Health’s implementation of the nurse redeployment program. While the idea behind workforce redeployment is intuitive (i.e., resource pooling), its implementation raises several key operations management (OM) challenges, including network design, advance-notice deployment decisions, and planning under demand uncertainty. We elaborate on each of these elements below, which is broadly relevant to hospital systems facing similar staffing shortages.

The **first element** is network design. Given the statewide distribution of hospitals, two structures are possible. The current model at IU Health follows a hub-and-spoke design (Števárová and Badánik 2018), where nurses travel between central and rural hospitals and return home the same day. An alternative is a fully connected (or point-to-point) network (Cook and Goodwin 2008), allowing deployments between any hospitals, including rural-to-rural ones. IU Health has been actively exploring this design to increase flexibility and better respond to asynchronous demand surges across regions. However, longer distances between rural sites make daily commuting impractical, which leads to the second design element.

The **second element** involves accounting for long-distance redeployments through advance notice and secondments. *Secondment* refers to a multi-day assignment at the receiving hospital, during which the nurse remains on-site to avoid prolonged and potentially hazardous daily commutes. It often comes with additional pay to compensate for remote travel.

IU Health initially implemented a real-time redeployment model, where decisions were made on the day of need, e.g., at 5 am each day before the morning shifts start. However, participation was minimal, as nurses were unwilling to engage without adequate notice. This led to the development of a two-stage framework: during the on-call planning phase (two weeks in advance), tentative assignments are made to provide nurses with early notification; during the deployment phase (each morning), these plans can be revised, either by canceling the planned deployment (with a cancellation fee) or initiating emergency deployment (at a premium cost).

This redesign highlights the *human-centric* nature of the problem: nurses are not items, unlike in traditional inventory transshipment or physical resource repositioning models (e.g., Shu et al. 2013, and He et al. 2020). Operational plans must incorporate advance notice, consider the travel burden, and account for the cost of modifying the plans. Nurses are also not interchangeable physical resources—each nurse has a home location. Nurses need to return to their home location after the secondment, making this fundamentally different from a network flow problem. Detailed discussion on the difference from the transshipment and repositioning literature is in Section 2. Secondment further complicates the problem structure by introducing temporal dependencies within the deployment phase; that is, a decision to deploy a nurse today affects their availability for multiple future

days. This necessitates a multi-stage decision problem with interdependent constraints across time. The resulting complexity exceeds what ad hoc or manual planning can effectively manage, calling for new analytical tools to support efficient nurse redeployment planning.

The resulting multi-stage problem naturally fits into a stochastic dynamic programming framework. This introduces the **third element**: how to make decisions under demand uncertainty, especially when assignments must be made up to two weeks in advance, before actual demand is observed. A common approach is the sample average approximation (SAA), which relies on historical data to estimate future demand. However, SAA becomes unreliable during disruptive events like a pandemic, where demand is highly non-stationary. This challenge is amplified in our human-centric setting: both understaffing and unnecessary travels can lead to negative consequences for nurse well-being and patient outcomes (Meredith et al. 2024). As such, the model must account for adverse scenarios, not just average-case performance.

1.2. Overview and Contributions

We make contributions across modeling, analytical framework, and operational insights.

First, we formulate a new multi-stage stochastic optimization model to support nurse redeployment with advance notice and secondments, particularly, capturing temporal correlations induced by the secondments; see Section 3. This bridges the gap between practical nurse redeployment and the literature on transshipment and repositioning by incorporating human-centric constraints such as advance notice and multi-stage plan adjustments.

Second, to address dynamic decision-making under uncertain and non-stationary demand, we adopt the SRO framework that accounts for deviations from historical data or forecasts and improves the out-of-sample performance. To ensure tractability, we approximate the deployment policy using linear decision rules, which allow us to reformulate the problem as a linear optimization model (see Section 4). Additionally, we implement a rolling-horizon scheme to incorporate real-time demand updates across the planning horizon.

Third, we generate actionable insights from an extensive case study in Section 5. Among all design levers, network structure has the largest impact on system cost—fully connected networks outperform hub-and-spoke models by allowing direct transfers and reducing unnecessary routing. However, this benefit depends critically on secondment alignment: short secondments for long-distance deployments can lead to excessive travel costs, while overly long secondments reduce responsiveness to changing demand. We also show that the SRO approach improves performance primarily in environments with rapidly increasing demand or under-predicted demand by proactively allocating additional staff and reducing emergency deployments. These findings highlight the need to jointly consider network flexibility, secondment planning, and robust decision-making in workforce redeployment strategies.

2. Literature Review

Our research is related to two streams of research. The first stream of research, reviewed in Section 2.1, includes inventory transshipment and repositioning of physical resources such as vehicles. The second stream, reviewed in Section 2.2, relates to the healthcare staffing.

2.1. Transshipment and Repositioning

Inventory transshipment involves moving inventory stock across locations within the same echelon to meet local demand, and has been extensively studied; see Paterson et al. (2011) for a comprehensive survey. A typical assumption is that inventory is consumed upon meeting demand—once used, it exits the system. In contrast, our nurse redeployment problem involves “reusable” human resources. That is, nurses who are temporarily deployed to another location return to their home hospital after completing their secondment and become available again (with the dynamics of availability dependent on prior assignments, not consumptions). This introduces different state dynamics and temporal dependencies not present in traditional inventory models.

Repositioning of physical resources involves moving items across locations to rebalance supply and demand. Examples include the repositioning of vehicles (e.g., bicycles, cars, emergency vehicles), empty containers, and other mobile assets (Song and Dong 2014, Bélanger et al. 2019, and Xie et al. 2021). We focus on the vehicle repositioning literature, which studies how to relocate shared vehicles across stations to maintain service balance, as it is most relevant to our setting. This area has been extensively explored; see, for instance, Nair and Miller-Hooks (2011), Shu et al. (2013), Lu et al. (2018), and Benjaafar et al. (2022), which typically assume full knowledge of the demand distribution. More recent work considers uncertainty via robust optimization. Among them, the following two are the closest to our research.

Hao et al. (2020) address idle vehicle pre-allocation under uncertain demand and covariate information, using a distributionally robust optimization (DRO) framework with moment and covariate-based ambiguity sets. He et al. (2020) also use a DRO approach to study fleet repositioning in free-float vehicle-sharing systems under temporal demand uncertainty. Our work differs from them in several important ways. (i) He et al. (2020) assume that both customer trips and repositioning trips can be completed within a single period, with vehicle availability determined by when they are next used or relocated. Hao et al. (2020) focus on a single-period setting. In contrast, nurses in our setting are assigned to multi-day secondments, which introduces *intertemporal dependencies* that significantly expand the state space and increase problem complexity. (ii) Unlike vehicles, nurses are not identical units, in the sense that each nurse has a designated home hospital and must return after secondment. This makes their origin a key attribute in planning, and the traditional network flow problem solutions do not apply here due to the *non-interchangeable* nature. (iii) As discussed

earlier, nurse redeployment decisions must be communicated in advance to ensure preparedness and acceptance, unlike vehicle repositioning, which is typically decided and executed at the start of each period. This advance-notice requires a multi-stage planning structure with commitment and adjustment layers. (iv) We adopt a sample robust optimization (SRO) method that does not require knowledge of moment-based parameters, in contrast to the moment-based ambiguity sets used in Hao et al. (2020) and He et al. (2020). This allows us to deal with non-stationary demand without relying on parametric assumptions.

2.2. Healthcare Staffing

Healthcare staffing in specific hospital units and emergency departments (EDs) has been extensively studied; see, for example, Yom-Tov and Mandelbaum (2014), Cho et al. (2019), Ding et al. (2020), Prabhu et al. (2020), Razak et al. (2020) and Hu et al. (2025). Advanced planning for healthcare staff assignment across units has also been explored in Huh et al. (2013), Rath et al. (2023), Yao et al. (2024). Our work is most closely related to Yuan (2025) and Ryu and Jiang (2025). Yuan (2025) propose a multistage staffing strategy for a centralized service system with multiple downstream units. They first set long-term base staffing levels, then determine staffing from pooled or dedicated agency staff at the start of each contract period. The pooled agency staff, deployable across locations, resemble our inter-facility float nurses. Their model is a stylized queueing network solved via stochastic fluid approximation, assuming full knowledge of the demand distribution. In contrast, we focus on daily deployment decisions with richer operational features: (i) advance notice requirements before redeployment, (ii) home locations with distance-dependent transfer costs, and (iii) uncertain, non-stationary demand with an unknown distribution, addressed via SRO. Ryu and Jiang (2025) develop a two-stage staffing model for float pools *within* a hospital, where the first stage allocates staff across units and the float pool, and the second stage reassigns float nurses within a shift to meet realized demand. Our setting instead addresses cross-hospital floating, which introduces fundamentally different operational challenges, particularly the advance notice and multi-day secondments, which are not relevant in within-hospital float settings. Moreover, while Ryu and Jiang (2025) use a two-stage DRO model with moment constraints, we employ an SRO framework that avoids parametric and moment-based assumptions, making it better suited for non-stationary demand in multi-hospital networks.

Our study setting is based on the inter-facility float practice at IU Health, with two prior works studying this novel practice. Shi et al. (2022) use nurse redeployment as an application to demonstrate their workload prediction framework, but their focus is on predictive modeling rather than planned decisions. Helm et al. (2024) develop a stochastic optimization model for nurse transfer with one-day secondments, assuming accurate demand predictions. In contrast, our work

addresses multi-period redeployment under limited and uncertain demand information, explicitly accounting for prediction errors using an SRO framework. This allows for more robust and adaptive staffing decisions over time.

3. Model Formulation

In this section, we formulate the model for the nurse deployment problem. We consider a finite-horizon planning problem with the horizon length being T days. Assume that there are L hospitals (locations) in the network. Throughout the paper, we use $[\cdot]$ to represent the set of running indices; for example, $[L] = \{1, 2, \dots, L\}$ represents the set of locations.

The nurse demands are assumed to be random. Let $\xi_t^i \in \mathbb{R}$ be the nurse demand on day t at location i , where $i \in [L]$ and $t \in [T]$. Let $\boldsymbol{\xi}_t = [\xi_t^i, 1 \leq i \leq L]$ be the demand vector at all locations on day t , and $\boldsymbol{\xi}_{[t]} = (\boldsymbol{\xi}_1, \dots, \boldsymbol{\xi}_t)$ be the historical demands up to day t for $t \in [T]$. The uncertain demands observed over the entire planning horizon is a stochastic process, denoted as $\boldsymbol{\xi}_{[T]} = (\boldsymbol{\xi}_1, \dots, \boldsymbol{\xi}_T)$ with a joint probability distribution \mathbb{P} . Without loss of generality, we assume the support set of $\boldsymbol{\xi}$ is nonnegative, and the support set is given by

$$\Xi = \{\boldsymbol{\xi} \in \mathbb{R}^{L \times T} : \xi_t^i \geq 0, 1 \leq i \leq L, 1 \leq t \leq T\}.$$

The central planner (e.g., the resource nurse manager) determines how many nurses to deploy from one location to another through a two-step decision process. First, an initial planned decision, commonly referred to as the on-call decision in hospital practice, is made at the start of the planning horizon (before any demand is realized) to provide nurses with advance notice. Then, daily deployment adjustments are made based on observed demand.

The overall decision timeline is illustrated in Figure 2, and we elaborate on each step below. All notations are summarized in Table 4 in Appendix A. Throughout the paper, we use the terms “on-call decision” and “planned decision” interchangeably, as well as “nurse transfer” and “nurse (re)deployment.”

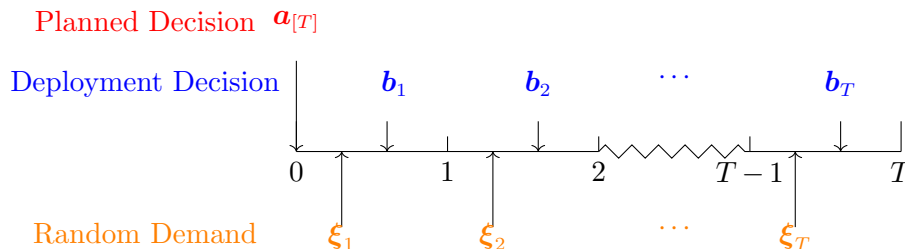


Figure 2 Timeline of the nurse transfer problem

Decision Variables. At the beginning of the planning horizon, the planner creates a tentative transfer plan—the *planned decision*—for the entire time horizon. Let a_t^{ij} denote the number of nurses tentatively planned to transfer from location i to location j on day t , where $i, j \in [L]$ and $t \in [T]$. By definition, we set $a_t^{ii} = 0$, as nurses are not transferred to their “home” location. For notational convenience, define $\mathbf{a}_t = [a_t^{ij}, 1 \leq i, j \leq L]$ as the vector of on-call decisions for day t , and $\mathbf{a}_{[t]} = (\mathbf{a}_1, \dots, \mathbf{a}_t)$ denote the sequence of on-call plans from day 1 to day t .

After observing the realized demand up to day t , the planner makes the *deployment decision*, determining the actual number of nurses to be transferred between locations on day t . Let b_t^{ij} denote the number of nurses deployed from location i to location j on day t , where $i, j \in [L]$. As before, we set $b_t^{ii} = 0$, and we define $\mathbf{b}_t = [b_t^{ij}, 1 \leq i, j \leq L]$ as the vector of deployment decisions for day t , and let $\mathbf{b}_{[t]} = (\mathbf{b}_1, \dots, \mathbf{b}_t)$ denote the sequence of deployment decisions up to day t . Importantly, each deployment decision b_t^{ij} is adapted to the realized demand information $\boldsymbol{\xi}_{[t]}$ observed up to day t .

Costs. When the nurses are planned to work at a location other than their home hospital, and the actual deployment occurs, they receive additional compensation. This includes a daily premium pay for working away from home and a relocation bonus upon transfer. Note that the deployed nurses are required to stay at the destination location for a minimum number of days, referred to as the *secondment*. The length of the secondment affects the incurred cost and it may vary depending on the travel distance and the timing within the planning horizon. Let $\mu^{ij}(t) = \omega^{ij} \wedge (T - t + 1)$ denote the secondment length for a nurse transferred from location i to location j on day t , where \wedge denotes the minimum operator. The parameter ω^{ij} represents the minimum required stay when sufficient time remains in the horizon; if the remaining number of days $(T - t + 1)$ is less than ω^{ij} , the nurse will stay at the destination hospital until the end of the planning horizon. Thus, the secondment length is given by the minimum of the two.

Let p denote the daily premium for working at a non-home location, and let τ^{ij} represent the additional compensation for traveling from location i to location j . The planned cost associated with the on-call decision \mathbf{a}_t on day t is given by:

$$c_t^p(\mathbf{a}_t) = \sum_{i=1}^L \sum_{j=1}^L (p\mu^{ij}(t) + \tau^{ij})a_t^{ij}, \quad (1)$$

which accounts for both the total premium pay over the secondment period and the one-time bonus per nurse transferred.

Once the deployment decision is made, it incurs a deployment cost consisting of three components: (i) emergency transfer cost, incurred when a transfer is initiated without prior notice; (ii) cancellation cost, incurred when a previously planned transfer is canceled; and (iii) shortage cost, incurred when local nurse demand exceeds available staffing. We specify each of these cost components more precisely below.

Emergency Transfer Cost. An emergency transfer occurs when the actual number of nurses deployed from location i to j on day t exceeds the planned (on-call) amount, i.e., when $b_t^{ij} > a_t^{ij}$. In such cases, the excess $(b_t^{ij} - a_t^{ij})$ nurses are deployed without advance notice and incur an additional cost. Let θ_t denote the premium multiplier applied to the daily wage p for emergency transfers on day t . The total emergency transfer cost for day t is given by:

$$\sum_{i=1}^L \sum_{j=1}^L (\theta_t p \mu^{ij}(t) + \tau^{ij})(b_t^{ij} - a_t^{ij})^+, \quad (2)$$

where $(x)^+ = \max\{x, 0\}$ denotes the positive part. This cost component accounts for the additional wage premiums (and travel bonuses) associated with emergency deployments.

Cancellation Cost. A cancellation occurs when a previously planned transfer is not executed, i.e., when $a_t^{ij} > b_t^{ij}$. In this case, $(a_t^{ij} - b_t^{ij})$ planned transfers are canceled, and each incurs a cancellation fee. We denote the percentage fee for canceling a planned transfer by η . The total cancellation cost for day t is given by:

$$\sum_{i=1}^L \sum_{j=1}^L (\eta - 1)(p \mu^{ij}(t) + \tau^{ij})(a_t^{ij} - b_t^{ij})^+, \quad (3)$$

which captures the lost travel bonuses and wages associated with canceling planned transfers.

Shortage Cost. We use δ_t^i to denote the imbalance between the demand and available nurses at location i on day t :

$$\delta_t^i = \xi_t^i - \left(K^i - \sum_{j=1}^L \sum_{k=(t-\omega^{ij}+1) \vee 1}^t b_k^{ij} + \sum_{j=1}^L \sum_{k=(t-\omega^{ji}+1) \vee 1}^t b_k^{ji} \right), \quad (4)$$

where K^i is the initial nurse capacity at location i , \vee denotes the maximum operator, $\sum_{j=1}^L \sum_{k=(t-\omega^{ij}+1) \vee 1}^t b_k^{ij}$ represents the number of nurses from location i who are still on secondment elsewhere on day t , and $\sum_{j=1}^L \sum_{k=(t-\omega^{ji}+1) \vee 1}^t b_k^{ji}$ represents the number of nurses from other locations who are currently on secondment at location i . Then, $(\delta_t^i)^+$ corresponds to the nurse shortage (understaffing) at location i on day t , which occurs when available staffing falls short of local demand ξ_t^i . Let s_t^i be the unit cost of shortage at location i on day t . Then, the total shortage cost incurred on day t is $\sum_{i=1}^L s_t^i (\delta_t^i)^+$.

In summary, the total deployment cost incurred on day t is given by

$$c_t^d(\mathbf{a}_t, \mathbf{b}_t, \boldsymbol{\xi}_t) = \sum_{i=1}^L \sum_{j=1}^L (\theta_t p \mu^{ij}(t) + \tau^{ij})(b_t^{ij} - a_t^{ij})^+ + \sum_{i=1}^L \sum_{j=1}^L (\eta - 1)(p \mu^{ij}(t) + \tau^{ij})(a_t^{ij} - b_t^{ij})^+ + \sum_{i=1}^L s_t^i (\delta_t^i)^+. \quad (5)$$

State Transitions. Before presenting the optimization formulation, we need to describe the state transitions. These transitions are much more complicated than those in the transshipment

or repositioning literature due to the secondment requirement and the fact that nurses are non-interchangeable—each has a designated home location and must return after deployment. As a result, we must explicitly track the number of deployed nurses by both their origin-destination pair and the remaining duration of their secondment.

Let $z_t^{ij}(k)$ be the number of nurses transferred from location i to location j , having the number of remaining secondment days as k at the beginning of day t (before the actual transfer), $1 \leq k \leq \omega - 1$, where $\omega = \max_{i,j} \omega^{ij}$. Let

$$\mathbf{z}_t = [z_t^{ij}(k), 1 \leq i, j \leq L, 1 \leq k \leq \omega - 1].$$

It is easy to see that $\mathbf{z}_1 = \mathbf{0}_{L \times L \times (\omega-1)}$. After observing the demand $\boldsymbol{\xi}_t$ on day t , the planner makes the deployment decision \mathbf{b}_t . Then on day $t + 1$ ($1 \leq t \leq T - 1$), we have

$$\begin{aligned} z_{t+1}^{ij}(k) &= z_t^{ij}(k+1) + b_t^{ij} \mathbb{1}_{\mu^{ij}(t)=k+1}, \quad 1 \leq i, j \leq L, 1 \leq k \leq \omega - 2, \\ z_{t+1}^{ij}(\omega - 1) &= b_t^{ij} \mathbb{1}_{\mu^{ij}(t)=\omega}, \quad 1 \leq i, j \leq L. \end{aligned} \quad (6)$$

It should be noted that $\mathbf{z}_{T+1} = \mathbf{0}_{L \times L \times (\omega-1)}$ since the nurses will return to their home location by the end of planning horizon.

Using \mathbf{z}_t 's, we can rewrite the imbalance quantity at location i on day t as

$$\delta_t^i = \xi_t^i - \left(K^i - \sum_{j=1}^L \sum_{k=1}^{\omega-1} z_t^{ij}(k) - \sum_{j=1}^L b_t^{ij} + \sum_{j=1}^L \sum_{k=1}^{\omega-1} z_t^{ji}(k) + \sum_{j=1}^L b_t^{ji} \right). \quad (7)$$

3.1. Optimization Formulation

The planned decision $\mathbf{a}_{[T]}$ is made at the beginning of the planning horizon, before any demand realization. Subsequently, on each day t , the deployment decision \mathbf{b}_t is optimized sequentially based on realized demand and the pre-specified plan. Let $v_t(\mathbf{a}_{[T]}, \mathbf{z}_t)$ denote the optimal expected cost from day t to the end of the horizon, given the advance plan $\mathbf{a}_{[T]}$ and the state \mathbf{z}_t . Without loss of generality, we set the terminal cost as $v_{T+1}(\mathbf{a}_{[T]}, \mathbf{z}_T) = 0$. This results in a nested optimization structure, where the outer problem determines the on-call plan:

$$\min_{\mathbf{a}_{[T]}} \sum_{t=1}^T c_t^p(\mathbf{a}_t) + v_1(\mathbf{a}_{[T]}, \mathbf{z}_1) \quad (8)$$

$$\text{s.t.} \quad \sum_{j=1}^L a_t^{ij} \leq K^i - \sum_{j=1}^L \sum_{k=(t-\omega^{ij}+1) \vee 1}^{t-1} a_k^{ij}, \quad 1 \leq i \leq L, 1 \leq t \leq T, \quad (9)$$

$$a_t^{ij} \geq 0, \quad 1 \leq i, j \leq L, 1 \leq t \leq T. \quad (10)$$

Constraint (9) is the capacity constraint – it ensures that the number of nurses planned for transfer from location i on day t does not exceed the number available at that location, accounting for those already on secondment.

The inner problem is solved recursively through dynamic programming. Given $\mathbf{a}_{[T]}$ and state \mathbf{z}_t , the expected cost-to-go function is:

$$v_t(\mathbf{a}_{[T]}, \mathbf{z}_t) = \mathbb{E} v_t^\xi(\mathbf{a}_{[T]}, \mathbf{z}_t, \boldsymbol{\xi}_t),$$

where v_t^ξ is defined as the solution to the following problem (for realized ξ_t):

$$v_t^\xi(\mathbf{a}_{[T]}, \mathbf{z}_t, \boldsymbol{\xi}_t) = \min_{\mathbf{b}_t} c_t^d(\mathbf{a}_t, \mathbf{b}_t, \boldsymbol{\xi}_t) + v_{t+1}(\mathbf{a}_{[T]}, \mathbf{z}_{t+1}) \quad (11)$$

$$\text{s.t. } \sum_{j=1}^L b_t^{ij} \leq K^i - \sum_{j=1}^L \sum_{k=1}^{\omega-1} z_t^{ij}(k), \quad 1 \leq i \leq L, \quad (12)$$

$$z_{t+1}^{ij}(k) = z_t^{ij}(k+1) + b_t^{ij} \mathbb{1}_{\mu^{ij}(t)=k+1}, \quad 1 \leq i, j \leq L, 1 \leq k \leq \omega-2, \quad (13)$$

$$z_{t+1}^{ij}(\omega-1) = b_t^{ij} \mathbb{1}_{\mu^{ij}(t)=\omega}, \quad 1 \leq i, j \leq L, \quad (14)$$

$$b_t^{ij} \geq 0, \quad 1 \leq i, j \leq L. \quad (15)$$

Constraint (12) is the capacity constraint for the inner problem. It ensures that deployment decisions do not exceed the number of nurses currently available at their home location, after accounting for those already on assignment.

Note that nurses are not transferred to their home location, and such transfers do not affect costs or feasibility. Thus, by construction, we have: $a_t^{ii} = b_t^{ii} = z_t^{ii}(k) = 0, \forall i \in [L], t \in [T], k \in [\omega-1]$, and these terms are excluded from the optimization model.

3.2. Stochastic Programming Formulation

The nurse transfer problem can also be formulated as a multi-stage stochastic optimization model. In this formulation, the deployment decision $\mathbf{b}_t(\boldsymbol{\xi}_{[t]})$ specifies a decision rule that determines the actual nurse transfers to be made on day t as a function of all the realized demand on or before day t , $\boldsymbol{\xi}_{[t]}$. With this decision rule definition, we formulate the following stochastic optimization programming.

$$\begin{aligned}
& \min_{\substack{\mathbf{a}_{[T]}, \\ \mathbf{b}_{[T]}(\boldsymbol{\xi}_{[T]})}} \sum_{t=1}^T \sum_{i=1}^L \sum_{j=1}^L (p\mu^{ij}(t) + \tau^{ij}) a_t^{ij} + \mathbb{E} \left(\sum_{t=1}^T \sum_{i=1}^L \sum_{j=1}^L \left((\theta_t p\mu^{ij}(t) + \tau^{ij}) (b_t^{ij}(\boldsymbol{\xi}_{[t]}) - a_t^{ij})^+ + \right. \right. \\
& \quad \left. \left. (\eta - 1)(p\mu^{ij}(t) + \tau^{ij})(a_t^{ij} - b_t^{ij}(\boldsymbol{\xi}_{[t]}))^+ \right) + \sum_{t=1}^T \sum_{i=1}^L s_t^i (\delta_t^i(\boldsymbol{\xi}_{[t]}))^+ \right) \\
& \text{s.t.} \quad \sum_{j=1}^L \sum_{k=(t-\omega^{ij}+1) \vee 1}^t a_k^{ij} \leq K^i, \quad 1 \leq i \leq L, 1 \leq t \leq T, \\
& \quad \sum_{j=1}^L \sum_{k=(t-\omega^{ij}+1) \vee 1}^t b_k^{ij}(\boldsymbol{\xi}_{[k]}) \leq K^i, \quad 1 \leq i \leq L, 1 \leq t \leq T, \\
& \quad \delta_t^i(\boldsymbol{\xi}_{[t]}) = \xi_t^i - \left(K^i - \sum_{j=1}^L \sum_{k=(t-\omega^{ij}+1) \vee 1}^t b_k^{ij}(\boldsymbol{\xi}_{[k]}) + \sum_{j=1}^L \sum_{k=(t-\omega^{ji}+1) \vee 1}^t b_k^{ji}(\boldsymbol{\xi}_{[k]}) \right), 1 \leq t \leq T, 1 \leq i \leq L, \\
& \quad a_t^{ij}, b_t^{ij}(\boldsymbol{\xi}_{[t]}) \geq 0, \quad 1 \leq i, j \leq L, 1 \leq t \leq T.
\end{aligned} \tag{16}$$

One major challenge in applying the stochastic optimization model is that the nurse demand distribution is seldom known in practice. One approach is to apply SAA to solve Problem (16) by approximating the demand distribution using the empirical distribution of $\boldsymbol{\xi}_{[T]}$. However, SAA exhibits poor out-of-sample performance when there are deviations from historical data or predictions, as is often the case with nurse demand during the COVID-19 pandemic (Bertsimas et al. 2022). To address this issue, we adopt the sample robust optimization approach to obtain a robust solution to the nurse transfer problem in Section 4.

4. Sample Robust Optimization Approach

In this section, we present the sample robust optimization approach to the multi-period nurse transfer problem. Compared to conventional sample average approximation, the sample robust approach incorporates potential deviations from available data samples to improve out-of-sample performance. This would allow better staffing decisions in the presence of demand ambiguity. We introduce the uncertainty set for sample deviations in Section 4.1 and the corresponding sample robust optimization model in Section 4.2. To address the computational challenge, we employ the linear decision rule and show a tractable reformulation in Section 4.3. For practical implementation, we further develop a rolling horizon approach in Section 4.4.

4.1. Uncertainty Set for Sample Deviation

Assume the true distribution \mathbb{P} of the uncertain nurse demand $\boldsymbol{\xi}_{[T]}$ is unknown. There are N available sample paths $\boldsymbol{\xi}_{[T]}^1, \boldsymbol{\xi}_{[T]}^2, \dots, \boldsymbol{\xi}_{[T]}^N$. Each sample path consists of nurse demands across all locations over T periods. We refer to the available demand data as sample paths, though they can also be predictions generated using historical data.

To incorporate potential perturbations of the realized demand from historical samples or predictions, we construct an uncertainty set \mathcal{U}_N^n around each available sample $\xi_{[T]}^n$ for $n = 1, \dots, N$,

$$\mathcal{U}_N^n = \{\zeta_{[T]} \in \Xi : \|\zeta_{[T]} - \xi_{[T]}^n\|_\infty \leq \epsilon_N\}. \quad (17)$$

Note that both $\zeta_{[T]}$ and $\xi_{[T]}^n$ are $L \times T$ matrices, of which each column represents the demand vector on a particular day. The matrix norm $\|\cdot\|_\infty$ is the entry-wise infinity norm, which is equal to the infinity norm of the vectorized form of the matrix. In (17), the potential realized demand $\zeta_{[T]}$ lies within an infinity-norm ball centered at the available sample $\xi_{[T]}^n$ with radius ϵ_N . The uncertainty set radius ϵ_N , which we also refer to as the *robust parameter*, determines the level of conservativeness of the robust model. A larger ϵ_N incorporates larger deviations from the available samples and, therefore, generates more conservative solutions. The choice of ϵ_N also depends on the sample size N . A larger sample provides more accurate demand distribution information, and consequently, one can choose a smaller ϵ_N . Note that we adopt the infinity norm primarily for tractability, as it allows an exact reformulation of the robust model, which we detail later. While alternative norms yield similar managerial insights, they often lead to intractable or overly conservative formulations with significantly higher computational costs. Thus, the infinity norm offers a practical and efficient choice for our application context. It has also been advocated in the literature (e.g., Jiang and Guan 2018, Bertsimas et al. 2019, and Wang et al. 2024).

For each $n = 1, \dots, N$, the uncertainty set in (17) is equivalent to $\xi_t^{i,n} - \epsilon_N \leq \zeta_t^i \leq \xi_t^{i,n} + \epsilon_N$, for all $t = 1, \dots, T$ and $i = 1, \dots, L$. For ease of notation, let $\underline{\zeta}_t^{i,n} = \xi_t^{i,n} - \epsilon_N$, $\bar{\zeta}_t^{i,n} = \xi_t^{i,n} + \epsilon_N$, $\underline{\zeta}_t^n = [\underline{\zeta}_t^{i,n}, 1 \leq i \leq L]$, and $\bar{\zeta}_t^n = [\bar{\zeta}_t^{i,n}, 1 \leq i \leq L]$.

4.2. Sample Robust Optimization Model

In the sample robust optimization model, we minimize the average of the worst-case costs under each uncertainty set, which is formulated as

$$\begin{aligned} \min_{\substack{a_{[T]}, \\ b_{[T]}(\zeta_{[t]})}} & \sum_{t=1}^T \sum_{i=1}^L \sum_{j=1}^L (p\mu^{ij}(t) + \tau^{ij})a_t^{ij} + \frac{1}{N} \sum_{n=1}^N \sup_{\zeta_{[T]} \in \mathcal{U}_N^n} \left(\sum_{t=1}^T \sum_{i=1}^L \sum_{j=1}^L \left((\theta_t p\mu^{ij}(t) + \tau^{ij})(b_t^{ij}(\zeta_{[t]}) - a_t^{ij})^+ + \right. \right. \\ & \left. \left. (\eta - 1)(p\mu^{ij}(t) + \tau^{ij})(a_t^{ij} - b_t^{ij}(\zeta_{[t]}))^+ \right) + \sum_{t=1}^T \sum_{i=1}^L s_t^i (\delta_t^i(\zeta_{[t]}))^+ \right) \\ \text{s.t.} & \sum_{j=1}^L \sum_{k=(t-\omega^{ij}+1) \vee 1}^t a_k^{ij} \leq K^i, \quad 1 \leq i \leq L, 1 \leq t \leq T, \\ & \sum_{j=1}^L \sum_{k=(t-\omega^{ij}+1) \vee 1}^t b_k^{ij}(\zeta_{[k]}) \leq K^i, \quad 1 \leq i \leq L, 1 \leq t \leq T, \\ & \delta_t^i(\zeta_{[t]}) = \zeta_t^i - \left(K^i - \sum_{j=1}^L \sum_{k=(t-\omega^{ij}+1) \vee 1}^t b_k^{ij}(\zeta_{[k]}) + \sum_{j=1}^L \sum_{k=(t-\omega^{ji}+1) \vee 1}^t b_k^{ji}(\zeta_{[k]}) \right), 1 \leq t \leq T, 1 \leq i \leq L, \end{aligned} \quad (18)$$

$$a_t^{ij}, b_t^{ij}(\zeta_{[t]}) \geq 0, \quad 1 \leq i, j \leq L, 1 \leq t \leq T,$$

$$\forall \zeta_{[T]} \in \mathcal{U}_N^n, 1 \leq n \leq N.$$

The nonlinear terms in (18) can be linearized, which we present in the following proposition. Specifically, we introduce two auxiliary variables $x_t^{ij}(\zeta_{[t]}) = (b_t^{ij}(\zeta_{[t]}) - a_t^{ij}(\zeta_{[t]}))^+$, and $y_t^i(\zeta_{[t]}) = (\delta_t^i(\zeta_{[t]}))^+$. Note that exact linearization is due to the use of the infinity norm in the uncertainty set in (17). Under other norms, similar linearization will result in more conservative reformulations.

PROPOSITION 1. *Problem (18) is equivalent to the following optimization problem.*

$$\begin{aligned} \min_{\substack{\mathbf{a}_{[T]}, \\ \mathbf{b}_{[T]}(\zeta_{[T]}), \\ \mathbf{x}_{[T]}(\zeta_{[T]}), \\ \mathbf{y}_{[T]}(\zeta_{[T]})}} \quad & \sum_{t=1}^T \sum_{i=1}^L \sum_{j=1}^L (p\mu^{ij}(t) + \tau^{ij}) a_t^{ij} + \frac{1}{N} \sum_{n=1}^N \sup_{\zeta_{[T]} \in \mathcal{U}_N^n} \left(\sum_{t=1}^T \sum_{i=1}^L \sum_{j=1}^L \left((\theta_t p\mu^{ij}(t) + \tau^{ij}) x_t^{ij}(\zeta_{[t]}) + \right. \right. \\ & \left. \left. (\eta - 1)(p\mu^{ij}(t) + \tau^{ij})(x_t^{ij}(\zeta_{[t]}) - b_t^{ij}(\zeta_{[t]}) + a_t^{ij}) \right) + \sum_{t=1}^T \sum_{i=1}^L s_t^i y_t^i(\zeta_{[t]}) \right) \end{aligned} \quad (19a)$$

$$\text{s.t.} \quad \sum_{j=1}^L \sum_{k=(t-\omega^{ij}+1) \vee 1}^t a_k^{ij} \leq K^i, \quad 1 \leq i \leq L, 1 \leq t \leq T, \quad (19b)$$

$$\sum_{j=1}^L \sum_{k=(t-\omega^{ij}+1) \vee 1}^t b_k^{ij}(\zeta_{[k]}) \leq K^i, \quad 1 \leq i \leq L, \quad (19c)$$

$$\zeta_t^i - \left(K^i - \sum_{j=1}^L \sum_{k=(t-\omega^{ij}+1) \vee 1}^t b_k^{ij}(\zeta_{[k]}) + \sum_{j=1}^L \sum_{k=(t-\omega^{ji}+1) \vee 1}^t b_k^{ji}(\zeta_{[k]}) \right) \leq y_t^i(\zeta_{[t]}), 1 \leq t \leq T, 1 \leq i \leq L, \quad (19d)$$

$$b_t^{ij}(\zeta_{[t]}) - a_t^{ij} \leq x_t^{ij}(\zeta_{[t]}), \quad 1 \leq t \leq T, 1 \leq i, j \leq L, \quad (19e)$$

$$a_t^{ij}, b_t^{ij}(\zeta_{[t]}), x_t^{ij}(\zeta_{[t]}) \geq 0, \quad 1 \leq i, j \leq L, 1 \leq t \leq T, \quad (19f)$$

$$y_t^i(\zeta_{[t]}) \geq 0, \quad 1 \leq i \leq L, 1 \leq t \leq T, \quad (19g)$$

$$\forall \zeta_{[T]} \in \mathcal{U}_N^n, 1 \leq n \leq N. \quad (19h)$$

The proof of Proposition 1 is in Appendix B.1.

4.3. Linear Decision Rule Reformulation

The adaptive decisions $b_t^{ij}(\zeta_{[t]})$, $x_t^{ij}(\zeta_{[t]})$ and $y_t^i(\zeta_{[t]})$ are all general functions of the past demand until day t , namely, $\zeta_{[t]}$. To achieve tractable, adaptive optimization, we employ the linear decision rule (LDR) approach; that is, we restrict the adaptive decisions to the class of affine functions of the demand realizations. In our problem, this means that the decisions $b_t^{ij}(\zeta_{[t]})$, $x_t^{ij}(\zeta_{[t]})$, and $y_t^i(\zeta_{[t]})$ are linear functions of $\zeta_{[t]}$.

The LDR of the deployment decision $\mathbf{b}_{[T]}$ is given by the following class of functions:

$$\mathcal{L}_b^{L^2 \times T} = \left\{ b_t^{ij}(\zeta_{[t]}) \in \mathcal{R}^{L \times t, 1}, t \in [T], i, j \in [L] \mid \begin{array}{l} \exists b_t^{0,ij}, b_{t,ml}^{1,ij} \in \mathbb{R}, m \in [t], l \in [L] : \\ b_t^{ij}(\zeta_{[t]}) = b_t^{0,ij} + \sum_{m=1}^t \sum_{l=1}^L b_{t,ml}^{1,ij} \zeta_m^l \end{array} \right\}. \quad (20)$$

In period t , from location i to j , $\mathcal{R}^{L \times t, 1}$ denotes the space of all measurable functions from $\mathbb{R}^{L \times t}$ to \mathbb{R}^1 , $b_t^{0,ij}$ is the intercept, and $b_{t,ml}^{1,ij}$ is the linear coefficient of the demand realization at location l in period m . Similarly, we have the LDR of $\mathbf{x}_{[T]}$ and $\mathbf{y}_{[T]}$ as follows.

$$\mathcal{L}_x^{L^2 \times T} = \left\{ x_t^{ij}(\boldsymbol{\zeta}_{[t]}) \in \mathcal{R}^{L \times t, 1}, t \in [T], i, j \in [L] \mid \begin{array}{l} \exists x_t^{0,ij}, x_{t,ml}^{1,ij} \in \mathbb{R}, m \in [t], l \in [L] : \\ x_t^{ij}(\boldsymbol{\zeta}_{[t]}) = x_t^{0,ij} + \sum_{m=1}^t \sum_{l=1}^L x_{t,ml}^{1,ij} \zeta_m^l \end{array} \right\}, \quad (21)$$

$$\mathcal{L}_y^{L \times T} = \left\{ y_t^i(\boldsymbol{\zeta}_{[t]}) \in \mathcal{R}^{L \times t, 1}, t \in [T], i \in [L] \mid \begin{array}{l} \exists y_t^{0,i}, y_{t,ml}^{1,i} \in \mathbb{R}, m \in [t], l \in [L] : \\ y_t^i(\boldsymbol{\zeta}_{[t]}) = y_t^{0,i} + \sum_{m=1}^t \sum_{l=1}^L y_{t,ml}^{1,i} \zeta_m^l \end{array} \right\}. \quad (22)$$

Using LDR, Problem (19) can be reformulated as a linear optimization problem, as outlined in the following proposition.

PROPOSITION 2. *Applying the linear decision rules, Problem (19) is equivalent to the following linear optimization problem.*

$$\begin{aligned} \min \quad & \sum_{t=1}^T \sum_{i=1}^L \sum_{j=1}^L (p\mu^{ij}(t) + \tau^{ij}) a_t^{ij} + \frac{1}{N} \sum_{n=1}^N \left(\sum_{t=1}^T \left(\sum_{l=1}^L \nu_{tl}^{epi} \bar{\zeta}_t^{ln} - \sum_{l=1}^L \psi_{tl}^{epi} \underline{\zeta}_t^{ln} \right) + \right. \\ & \left. \sum_{t=1}^T \sum_{i=1}^L \left(\sum_{j=1}^L \left((\theta_t p\mu^{ij}(t) + \tau^{ij}) x_t^{0,ij} + (\eta - 1)(p\mu^{ij}(t) + \tau^{ij})(x_t^{0,ij} - b_t^{0,ij} + a_t^{ij}) \right) - s_t^i y_t^{0,i} \right) \right) \\ \text{s.t.} \quad & \nu_{tl}^{epi} - \psi_{tl}^{epi} = \sum_{k=t}^T \sum_{i=1}^L \left(\sum_{j=1}^L \left((\theta_k p\mu^{ij}(k) + \tau^{ij}) x_{k,tl}^{1,ij} + (\eta - 1)(p\mu^{ij}(k) + \tau^{ij})(x_{k,tl}^{1,ij} - b_{k,tl}^{1,ij}) \right) \right. \\ & \left. + s_k^i y_{k,tl}^{1,i} \right), \quad 1 \leq l \leq L, 1 \leq t \leq T, \end{aligned}$$

capacity constraints (23),

shortage constraints (24),

emergency transfer constraints (25),

nonnegativity constraints (26),

where the capacity constraints are given by

$$\begin{aligned} & \sum_{j=1}^L \sum_{k=(t-\omega^{ij}+1) \vee 1}^t a_k^{ij} \leq K^i, \quad 1 \leq i \leq L, 1 \leq t \leq T, \\ & \sum_{k=1}^T \left(\sum_{l=1}^L \nu_{klti}^{cap} \bar{\zeta}_k^{ln} - \sum_{l=1}^L \psi_{klti}^{cap} \underline{\zeta}_k^{ln} \right) + \sum_{j=1}^L \sum_{k=(t-\omega^{ij}+1) \vee 1}^t b_k^{0,ij} \leq K^i, \quad 1 \leq i \leq L, 1 \leq t \leq T, 1 \leq n \leq N, \quad (23) \\ & \nu_{klti}^{cap} - \psi_{klti}^{cap} = \sum_{m=k}^T \sum_{j=1}^L \mathbb{1}_{\{(t-\omega^{ij}+1) \vee 1\} \leq m \leq t} b_{m,kl}^{1,ij} \zeta_k^l, \quad 1 \leq i \leq L, 1 \leq t \leq T, 1 \leq l \leq L, 1 \leq k \leq T; \end{aligned}$$

the shortage constraints are given by

$$\begin{aligned} \sum_{k=1}^T \left(\sum_{l=1}^L \nu_{klti}^{sho} \bar{\zeta}_k^{ln} - \sum_{l=1}^L \psi_{klti}^{sho} \zeta_k^{ln} \right) + \zeta_t^i - \left(K^i - \sum_{j=1}^L \sum_{k=(t-\omega^{ij}+1) \vee 1}^t b_k^{0,ij} + \sum_{j=1}^L \sum_{k=(t-\omega^{ji}+1) \vee 1}^t b_k^{0,ji} \right) &\leq y_t^{0,i}, \\ 1 \leq i \leq L, 1 \leq t \leq T, 1 \leq n \leq N, \\ \nu_{klti}^{sho} - \psi_{klti}^{sho} &= \sum_{m=k}^T \left(\sum_{j=1}^L \mathbb{1}_{\{(t-\omega^{ij}+1) \vee 1 \leq m \leq t\}} \sum_{l=1}^L b_{m,kl}^{1,ij} \zeta_k^l - \sum_{j=1}^L \mathbb{1}_{\{(t-\omega^{ji}+1) \vee 1 \leq m \leq t\}} \sum_{l=1}^L b_{m,kl}^{1,ji} \zeta_k^l - \right. \\ &\quad \left. \mathbb{1}_{\{m=t\}} \sum_{l=1}^L y_{m,kl}^{1,i} \zeta_k^l \right), \quad 1 \leq i, l \leq L, 1 \leq t \leq T, 1 \leq k \leq T; \end{aligned} \quad (24)$$

the emergency transfer constraints are given by

$$\begin{aligned} \sum_{k=1}^T \left(\sum_{l=1}^L \nu_{kltij}^{eme} \bar{\zeta}_k^{ln} - \sum_{l=1}^L \psi_{kltij}^{eme} \zeta_k^{ln} \right) + b_t^{0,ij} - a_t^{ij} &\leq x_t^{0,ij}, \quad 1 \leq i, j \leq L, 1 \leq t \leq T, 1 \leq n \leq N, \\ \nu_{kltij}^{eme} - \psi_{kltij}^{eme} &= \sum_{m=k}^T \mathbb{1}_{\{m=t\}} (b_{m,kl}^{1,ij} \zeta_m^l - x_{m,kl}^{1,ij} \zeta_m^l), \quad 1 \leq i, j, l \leq L, 1 \leq t \leq T, 1 \leq k \leq T; \end{aligned} \quad (25)$$

and the nonnegativity constraints are given by

$$\begin{aligned} a_t^{ij} &\geq 0, \quad 1 \leq i, j \leq L, 1 \leq t \leq T, \\ \sum_{k=1}^T \left(\sum_{l=1}^L \nu_{kltij}^{nnb} \bar{\zeta}_k^{ln} - \sum_{l=1}^L \psi_{kltij}^{nnb} \zeta_k^{ln} \right) &\leq b_t^{0,ij}, \quad 1 \leq i, j \leq L, 1 \leq t \leq T, 1 \leq n \leq N, \\ \nu_{kltij}^{nnb} - \psi_{kltij}^{nnb} &= - \sum_{m=k}^T \mathbb{1}_{\{m=t\}} b_{m,kl}^{1,ij} \zeta_m^l, \quad 1 \leq i, j, l \leq L, 1 \leq t \leq T, 1 \leq k \leq T, \\ \sum_{k=1}^T \left(\sum_{l=1}^L \nu_{kltij}^{nnx} \bar{\zeta}_k^{ln} - \sum_{l=1}^L \psi_{kltij}^{nnx} \zeta_k^{ln} \right) &\leq x_t^{0,ij}, \quad 1 \leq i, j \leq L, 1 \leq t \leq T, 1 \leq n \leq N, \\ \nu_{kltij}^{nnx} - \psi_{kltij}^{nnx} &= - \sum_{m=k}^T \mathbb{1}_{\{m=t\}} x_{m,kl}^{1,ij} \zeta_m^l, \quad 1 \leq i, j, l \leq L, 1 \leq t \leq T, 1 \leq k \leq T, \\ \sum_{k=1}^T \left(\sum_{l=1}^L \nu_{klti}^{nny} \bar{\zeta}_k^{ln} - \sum_{l=1}^L \psi_{klti}^{nny} \zeta_k^{ln} \right) &\leq y_t^{0,i}, \quad 1 \leq i \leq L, 1 \leq t \leq T, 1 \leq n \leq N, \\ \nu_{klti}^{nny} - \psi_{klti}^{nny} &= - \sum_{m=k}^T \mathbb{1}_{\{m=t\}} \sum_{l=1}^L y_{m,kl}^{1,i} \zeta_k^l, \quad 1 \leq i, l \leq L, 1 \leq t \leq T, 1 \leq k \leq T, \\ \nu^{epi}, \psi^{epi} &\in \mathbb{R}_+^{T \times L}, \nu^{cap}, \psi^{cap}, \nu^{sho}, \psi^{sho}, \nu^{nny}, \psi^{nny} \in \mathbb{R}_+^{T^2 \times L^2}, \nu^{eme}, \psi^{eme}, \nu^{nnb}, \psi^{nnb} \in \mathbb{R}_+^{T^2 \times L^3}. \end{aligned} \quad (26)$$

The proof of Proposition 2 is in Appendix B.2. The main idea of the proof is based on Bertsimas et al. (2023).

It should be noted that solutions generated using LDR are not necessarily feasible. Moreover, LDRs are typically not used directly as implementable policies in multi-stage optimization problems (Bertsimas et al. 2019). However, the LDR reformulation offers significant computational advantages. This enables one to re-optimize dynamically as new information becomes available, rather than committing to the LDR policy itself. In the next section, we introduce a rolling-horizon approach to implement this dynamic decision-making framework.

4.4. Rolling-Horizon Implementation

The rolling-horizon approach is a commonly used technique in practice that leverages the observed demand at the beginning of each day to re-optimize decisions over a fixed planning horizon, leading to improved outcomes. This method has been discussed in prior literature, including Chand et al. (2002) and Glomb et al. (2022). In this section, we describe the rolling-horizon approach for our specific context.

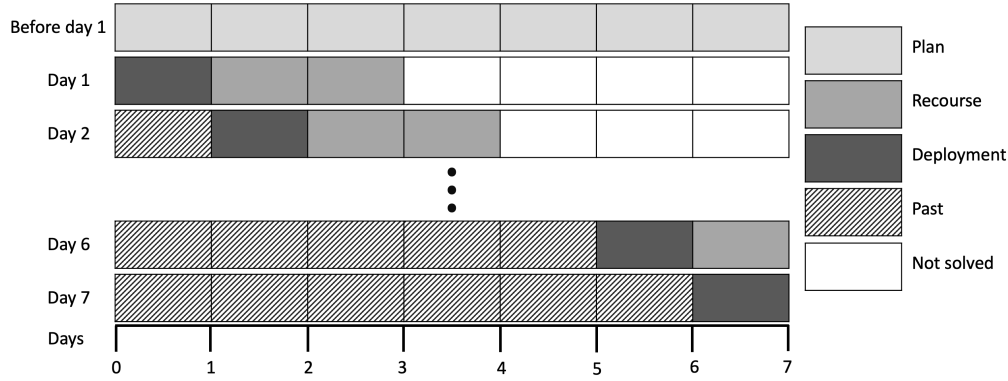


Figure 3 Schematic description of the rolling-horizon approach ($T = 7$ and $\omega = 3$)

Figure 3 illustrates the decision-making timeline. At the beginning of the planning horizon, we solve the reformulated problem in Proposition 2 to derive the planned decision. We denote the resulting optimal planned decision over the entire planning horizon by $\mathbf{a}_{[T]}^*$. These specify the planned transfer decisions for each day $t \in [T]$ and correspond to the light gray (Plan) blocks in Figure 3. Then, on each day t , we observe the realized demand ξ_t and re-solve the problem for the remaining horizon $[t, t + S(t) - 1]$ using updated demand information. This produces new recourse decisions $[\mathbf{b}_t^*, \dots, \mathbf{b}_{t+S(t)-1}^*]$. Only the first decision \mathbf{b}_t^* is implemented, while the rest are discarded. The dark gray (Deployment) and medium gray (Recourse) blocks in Figure 3 illustrate this process: each implemented deployment decision corresponds to the first block in the re-optimized sub-horizon, and the remaining blocks are not used. This rolling-horizon procedure continues until day T , at which point the problem becomes a deterministic optimization problem and the final-day recourse decision is directly implemented.

Feasibility is always guaranteed in this approach because only the first decision \mathbf{b}_t^* , optimized based on observed demand, is implemented. While future-stage decisions (e.g., $\mathbf{b}_{t+1}^*, \mathbf{b}_{t+2}^*$) are linear functions of yet-to-be-realized demand and may not remain feasible, they are not executed. This iterative process ensures that each deployed decision is always feasible given the current state.

We conclude this section by two remarks. First, we need to choose $S(t)$, the decision horizon, when implementing the approach. To balance between the increased computational cost due to a

longer horizon and the myopia caused by a shorter decision horizon, we set $S(t) = \omega \wedge (T - t + 1)$, the secondment length. Second, it is necessary to acquire an integer solution for the nurse transfer decisions in practice. One strategy involves enforcing integer constraints on the variables a_t^{ij} and b_t^{ij} . However, the computational complexity increases significantly, especially when dealing with a large number of locations or an extended planning horizon. Thus, we employ the randomized rounding approach (Raghavan and Thompson 1987) to round the fractional solutions $\mathbf{a}_{[T]}^*$, \mathbf{b}_1^* , \dots , \mathbf{b}_T^* . This approach keeps the computation tractable while maintaining a close approximation to the mixed-integer optimization problem (Hao et al. 2020).

5. Case Study

In this section, we present a case study to evaluate the effectiveness of our analytical framework. The study setting is inspired by the configuration of IU Health’s service regions, shown in Figure 1. To maintain generalizability and avoid attributing specific views, we refer to the system as an “anonymous hospital network” in the case study, with four hospitals distributed across four regions: West, East, South, and Central. Section 5.1 outlines the simulation platform used for performance evaluation, along with the parameter calibration process. Sections 5.2 and 5.3 focus on analyzing the impact of network design and secondment, respectively. In Section 5.4, we demonstrate the value of robust optimization by comparing solutions from the sample robust optimization with those from the sample average approximation.

5.1. Simulation Evaluation Platform

Figure 4 illustrates the data pipeline of the simulation evaluation platform, which consists of three key modules: a simulator that generates data, an optimization module that makes nurse transfer decisions and interacts with the simulator to execute those decisions, and an evaluation module that assesses the performance of the deployment strategies. Section 5.1.1 provides a detailed explanation of each module. Section 5.1.2 outlines the calibration of input parameters.

5.1.1. Platform Modules

Simulator. The first module of our platform simulates daily nurse demand for each hospital for given input parameters (such as daily arrival rate, discharge rate, etc.). The simulator primarily simulates patient movements within the network of hospitals, from which we derive the patient census in each unit at a given time. The nurse demand is then calculated from the patient census using the required nurse-to-patient ratio. Specifically, we consider three types of units in each hospital: medical-surgical unit (MS), progressive care unit (PCU), and intensive care unit (ICU). To estimate the patient census for each unit, we explicitly model patient transitions between MS, PCU, and ICU, patient discharges, and patient arrivals at each unit; detailed information on these

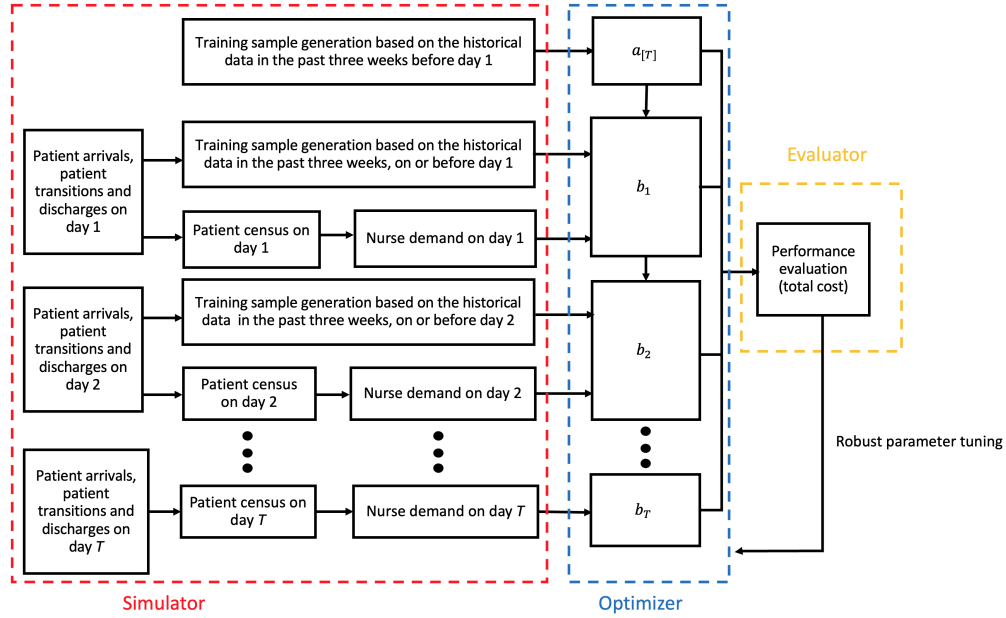


Figure 4 Data pipeline for simulation evaluation (For simplicity, we only show the optimization over one planning horizon for T days. If there are multiple planning horizons, the same approach applies).

processes is in Appendix C.1. Based on the estimated patient census, we apply the following nurse-to-patient ratio to calculate the nurse demand: 5:1 for MS, 3:1 for PCU, and 2:1 for ICU (Wolters Kluwer 2016).

The simulator is used to generate two types of demand data: *testing sample paths*, which are generated using the actual demand distribution (ground truth), and *training sample paths*, which are demand predictions generated based on testing sample paths. Note that the testing and training sample paths have different underlying demand distributions. This distinction allows us to incorporate potential deviations from historical samples or predictions and separate decision-making and decision-evaluation.

Optimizer. The optimizer makes planned decisions at the start of each week and deployment decisions on a daily basis. We consider a total horizon of $W = 27$ weeks (189 days). Before running the optimizer, we pre-generate $H = 30$ testing sample paths, representing sequences of historical demand realized in each of the L hospitals over W weeks. The testing data is generated by the simulator calibrated with real hospital data; see details of parameter calibration in Section 5.1.2.

The optimizer is executed on each of the H testing sample paths, treating each path as an independent evaluation instance. In each iteration, for every week $w \in [1, W]$ and each day t within that week, we estimate the arrival rates, unit transition probabilities, and discharge probabilities for each hospital using the demand from the previous three weeks. These estimates, which can differ from the true parameters, are then used to generate the training sample paths used in the sample-robust optimization model.

On each day t , we generate $\hat{H} = 25$ training sample paths. If day t is the starting day of a week, the weekly planned decisions \mathbf{a} are first optimized using the training sample paths. Then, for each day in that week, the deployment decisions \mathbf{b}_t are optimized via a rolling-horizon approach, as described in Section 4. Note that the training sample paths are also generated in a rolling-horizon manner to reflect evolving estimates and maintain consistency with the “rolling” decision; see Figure 4 for an illustration. Additional implementation details are provided in Appendix C.2.

Evaluator. The performance evaluation module is designed to assess the performance of the planned and deployment decisions on the testing data for a given optimization method \mathcal{A} . Method \mathcal{A} can refer to either the SRO or the SAA approach (where SAA is a special case of SRO with the robustness parameter set to zero). Evaluation is performed on $H = 30$ testing instances. Under each of the instance, we generate $\hat{H} = 25$ training sample paths, each containing nurse demand across L locations and $T = 7$ days. In the SRO method, we group every 5 training sample paths into one training set, resulting in $M = 5$ training sets per instance. For consistency, we apply the same grouping structure to the SAA method.

Let $\mathbf{a}_{m,h,w}^{\mathcal{A}*}$ ($\mathbf{b}_{m,h,w}^{\mathcal{A}*}$) denote the optimal planned (deployment) decision in week w using method \mathcal{A} under training data m and testing sample path h , where $m \in [M]$, $h \in [H]$, $w \in \{1, 2, \dots, W\}$. Then we compute the out-of-sample cost in week w using method \mathcal{A} as follows:

$$V_w^{\mathcal{A}} = \frac{1}{MH} \sum_{m=1}^M \sum_{h=1}^H \left(\sum_{t=1}^T \sum_{i=1}^L \sum_{j=1}^L (p\mu^{ij}(t) + \tau^{ij}) a_{m,h,w,t}^{\mathcal{A},ij} + \sum_{t=1}^T \sum_{i=1}^L \sum_{j=1}^L \left((\theta_t p\mu^{ij}(t) + \tau^{ij}) (b_{m,h,w,t}^{\mathcal{A},ij} - a_{m,h,w,t}^{\mathcal{A},ij})^+ + (\eta - 1)(p\mu^{ij}(t) + \tau^{ij})(a_{m,h,w,t}^{\mathcal{A},ij} - b_{m,h,w,t}^{\mathcal{A},ij})^+ \right) + \sum_{t=1}^T \sum_{i=1}^L s_t^i (\delta_{m,h,w,t}^{\mathcal{A},i})^+ \right), \quad (27)$$

where $\delta_{m,h,w,t}^{\mathcal{A},i}$ represents the demand-staffing imbalance on day t in week w using method \mathcal{A} , training set m , and testing sample path h . The average cost over the total horizon with W weeks by using method \mathcal{A} is given by

$$V^{\mathcal{A}} = \frac{1}{W} \sum_{w=1}^W V_w^{\mathcal{A}}. \quad (28)$$

5.1.2. Parameter Calibration In this section, we provide the details on the parameters utilized in our analysis. For ease of exposition, we index the four hospitals (West, East, South, and Central) with numeric values – hospital 1, 2, 3, and 4, respectively.

Patient Flow Parameters. The key input to the simulator are the number of patient arrivals, discharges, and transitions between units within the hospital. To generate the ground-truth (testing) demand, we begin by estimating baseline arrival rates using historical data from an anonymous hospital system. Temporal and spatial correlations are then introduced through an autoregressive model with noise terms designed to capture these dependencies. Note that the baseline rates and correlation structures are estimated from data, while the arrival model is parameterized to allow

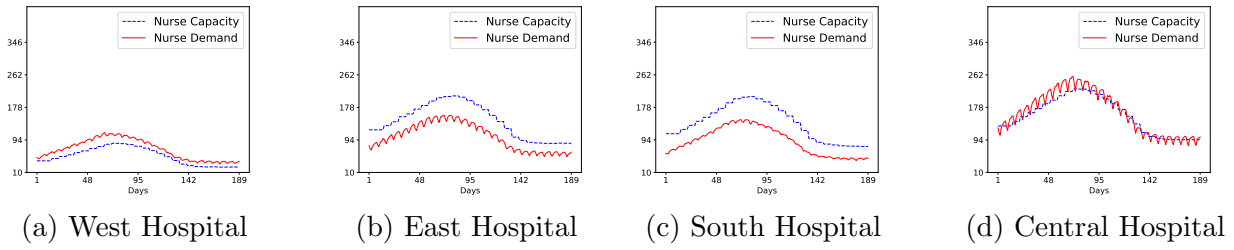


Figure 5 Daily nurse demand and capacity at each hospital

tuning of hyperparameters. This enables us to simulate demand surges—such as peak census levels observed during the COVID-19 pandemic—using publicly available benchmarks from the American Hospital Directory (2024). See details in Appendix C.1.

Figure 5 illustrates the average nurse demand under the baseline testing scenarios over the $W = 27$ weeks at four hospitals, alongside their respective nurse capacities. The demand trajectory in this baseline follows three phases: an increasing demand phase, a decreasing demand phase, and a stable demand phase. Nurse capacity at each hospital is estimated using the provided budgeted staffing ratio and is adjusted weekly to approximate the corresponding trends in demand. Notably, West and Central Hospitals consistently face staffing shortages, while East and South Hospitals maintain surplus nurse capacity. This structural imbalance creates an opportunity for nurse transfers across hospitals, using the redeployment strategies to mitigate system-wide shortages.

Cost Parameters. We use a daily payment premium $p = 1$ as the baseline and normalize other costs accordingly. We set the cancellation fee percentage at 5%, and the daily salary premium multiplier for emergency transfer θ_t at 1.6. We set the non-salary transfer cost (reimbursement for nurses who travel to a remote hospital), τ_{ij} , based on the geographical distance between different hospitals, $i, j \in [L]$. Our secondment setting is also based on the distance between locations, with longer distances resulting in longer secondments. Specifically, secondments between nearby locations (e.g., West and Central, East and Central) have a duration of 1 day, while those between more distant locations (e.g., West and East, West and South) have a duration of 2 days, due to logistical challenges. This is referred to as the base secondment scenario. Table 1 summarizes the parameters.

To incentivize hospitals to opt for emergency transfers instead of enduring nurse shortages (particularly when nurses are available at other healthcare facilities), we need to ensure that the unit shortage cost s_t^i exceeds the total emergency cost incurred by the emergency transfer. We set $s_t^i = 15$ that is greater than the maximum emergency transfer cost.

Within our study, we determine the robust parameter for week w as follows. For the first week, we set the robust parameter $\epsilon_{N,1}$ to zero. For week w ($w \geq 2$), we select the robust parameter

Hospital From/To	Parameters	West	East	South	Central
West	Cost	-	1.46	1.68	1.20
	Distance	-	88	110	62
	Secondment	-	2	2	1
East	Cost	1.46	-	1.70	1.14
	Distance	88	-	112	56
	Secondment	2	-	2	1
South	Cost	1.68	1.70	-	1.10
	Distance	110	112	-	52
	Secondment	2	2	-	1
Central	Cost	1.20	1.14	1.10	-
	Distance	62	56	52	-
	Secondment	1	1	1	-

Table 1 Transfer cost, transfer distance and secondment setting

$\epsilon_{N,w}$ by choosing the best-performing parameter from the set $\{(\epsilon_{N,w-1} - 5v)^+, (\epsilon_{N,w-1} - 5v)^+ + 5, (\epsilon_{N,w-1} - 5v)^+ + 10, \dots, \epsilon_{N,w-1} + 5v\}$ based on the results from week $w - 1$. Here, v can be adjusted to reflect changes in nurse demand. For example, we set $v = 2$ for the demand pattern described in Section 5.1.1, and increase it to $v = 5$ under scenarios with more pronounced demand changes described in Appendix D.4.

5.2. Network Structure

In this section, we evaluate the impact of network designs on the performance of the nurse redeployment program, comparing two structures: the hub-and-spoke (HS) network and the fully connected (FC) network. In the HS network, nurse transfers are restricted to occur between rural hospitals (West, East, and South – the spokes) and the Central Hospital (the hub), whereas the FC network allows transfers between any two locations. We use the *baseline secondment* scenario considering the long distances between rural areas, i.e., the secondment duration for transfers between spokes is set to two days, whereas the secondment for transfers between hub and spoke is one day; see Figure 6 for the network designs and the secondment settings. In addition, we consider two alternative secondment scenarios. One is the *one-day secondment* scenario, where all secondments are set to a duration of one day; the other one is the *three-day secondment* scenario, where the secondment between nearby locations is still one day, but the secondment between the locations with long distance is set as three days.

Table 2 compares the average (weekly) costs under the two designs, over the entire horizon, with different secondment scenarios and the two optimization methods. The results show a significantly lower total cost for the FC network (reduced by 23% to 35%), regardless of the method used. We also examine two additional performance metrics: the average number of nurse transfers and the average miles traveled (based on the distance between locations) per week across all locations. Table 2 shows that both metrics decrease significantly under the FC network (reduced by 13% to 52%), consistent with the lower costs compared to the HS network.

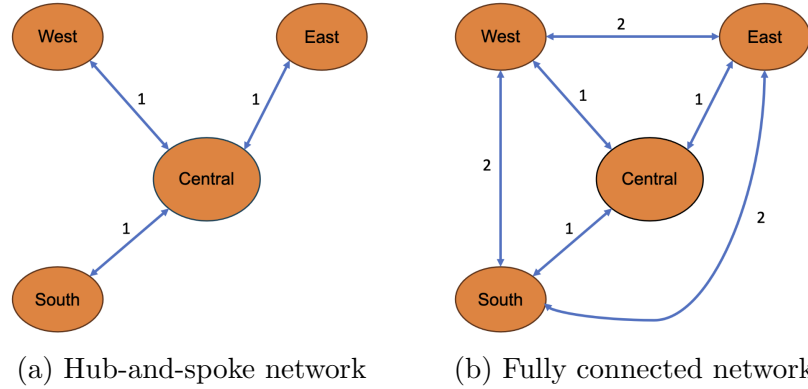


Figure 6 Baseline secondment setting under different network designs.

Table 2 Average cost, deployed transfers, and transferred miles per week for SAA and SRO across various network designs and secondment scenarios.

Metrics	Network design	Baseline secondment		One-day secondment		Three-day secondment	
		SAA	SRO	SAA	SRO	SAA	SRO
Cost	FC	641.90	633.05	713.30	702.20	607.52	606.98
	HS	933.35	914.71	-	-	-	-
Deployed transfers	FC	149.05	148.86	195.63	195.62	138.64	139.75
	HS	291.69	292.04	-	-	-	-
Transferred miles	FC	10137.89	10326.54	14159.54	14289.09	9309.35	9529.61
	HS	16399.95	16438.94	-	-	-	-

To explore the reasons behind the advantage demonstrated by the FC design, we analyze (i) the number of transfers from West, South, and East Hospitals to Central, and (ii) the number of transfers from Central, South and East to West, considering the nurse shortages at both West and Central Hospitals. Figure 7 shows that in the HS network, transfers occur from Central to West, with Central receiving nurses from South and East. In contrast, Figure 8 illustrates that in the FC network, nurses can be transferred directly between East and West, and from South to Central. A similar pattern is observed across different secondment scenarios and methods.

To summarize, the FC network outperforms the HS design in this setting for two key reasons. First, it enables direct transfers to hospitals with shortage (e.g., West), which avoids costly intermediary routing through the hub (Central). Second, it leverages longer secondments between distant hospitals (West, South, and East), which reduce average daily transfer costs, as the fixed costs such as relocation bonuses are spread over multiple days. Notably, the cost gap between the two network designs is more substantial than the differences observed across secondment scenarios or optimization methods, suggesting a dominant role of network structure. However, this does *not* imply that the FC design is universally superior. As we discuss next, its performance depends critically on the alignment between network structure and secondment policies.

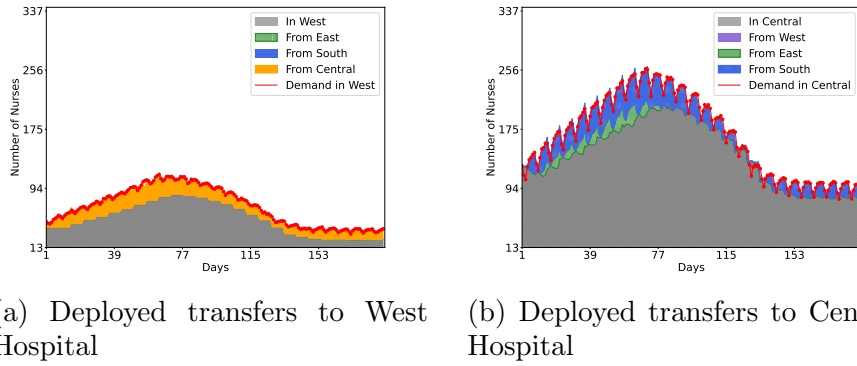


Figure 7 Daily deployed nurse transfers to West and Central Hospitals by using SRO under the hub-and-spoke (HS) network.

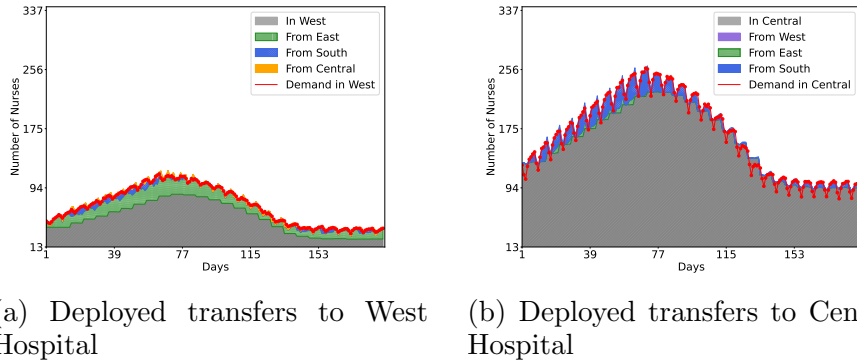


Figure 8 Daily deployed nurse transfers to West and Central Hospitals by using SRO under the base secondment scenario and fully connected (FC) network.

5.3. Effect of Secondment

In this section, we study the impact of secondment length. Our main finding is that, if secondment lengths are not properly adapted to the network structure, system performance can deteriorate. Specifically, assigning too short secondments to long-distance transfers may lead to excessive commuting costs or nurse fatigue, which counter-effects the benefit from the improved network connectivity (Section 5.3.1). Conversely, overly long secondments, while reducing the per-day fixed costs by spreading them out, can reduce responsiveness and limit the ability to reallocate staff when demand shifts (Section 5.3.2). Thus, secondment policies must be carefully calibrated to the network structure to balance efficiency, flexibility, and nurse well-being.

5.3.1. Interplay with Network Structure Under the baseline demand pattern, the FC network consistently outperforms the HS network across all settings. However, this advantage is not universal. In this section, we examine an alternative demand scenario in which only the West Hospital experiences a nurse shortage, while the other three hospitals have surplus capacity (see

details in Appendix D.1). Moreover, we assume that, under this setting, transfers are restricted to occur only between the West and Central Hospitals in the HS network, and between the West and South Hospitals in the FC network. As shown in Table 7 in Appendix D.1, when the secondment length for rural-to-rural transfers is set to one day, the HS network achieves lower total costs—359 (SAA) and 353 (SRO)—compared to the FC network’s 414 (SAA) and 409 (SRO). HS also results in shorter total transfer distances, with total transfer volumes comparable across both network structures. However, when the secondment length increases to two or more days, the FC network’s cost drops below 329, once again outperforming the HS network. The FC network also achieves a reduction in total transfer volume, although the total transfer distance may remain slightly higher than that of the HS network at a two-day secondment length.

These findings highlight the importance of allowing longer secondment durations when having rural-to-rural nurse transfers in the FC network. Moreover, the FC design introduces more complexity in coordination, as it requires nurses to travel to and work at more locations (and nurses need to be familiar with multiple workplaces). In Appendix D.2, we further analyze the impact of such coordination complexity—modeled as additional coordination costs—on the performance of both HS and FC networks.

5.3.2. Impact of Secondment Length In this section, we take a deep dive to investigate the impact of different secondment length, focusing on the fully connected (FC) network design. Under the baseline setting, we observe a monotonic decrease in total cost as the secondment length increases (Table 2). This trend is mainly driven by the relatively high base transfer cost (set at 1.1), which makes longer secondments more cost-effective by spreading the cost of relocation over multiple days. To explore the sensitivity of this trend, we reduce the transfer cost to one-tenth of its original value (0.1), following the calibration in Appendix C.3. Under this lower-cost setting, we uncover an interesting *U-shaped* relationship between secondment length and system cost.

Specifically, Table 3 reports the average weekly cost, number of actual nurse transfers, and total transfer mileage under varying secondment scenarios for both SAA and SRO methods (using the lower transfer cost). To isolate the impact of rural-to-rural secondments, we fix the secondment length from central to rural hospitals at one day while varying the rural-to-rural secondment length across 1, 3, and 7 days. We observe from the table that increasing secondment length from 1 to 3 days reduces costs, but extending it further to 7 days leads to an increase. This U-shaped cost pattern is further illustrated in Figure 9, which plots weekly cost trends under different secondment lengths for SAA and SRO.

These results indicate the existence of a “sweet spot” for optimal secondment duration. The underlying trade-off behind the U-shape is clear: shorter secondments result in high daily transfer

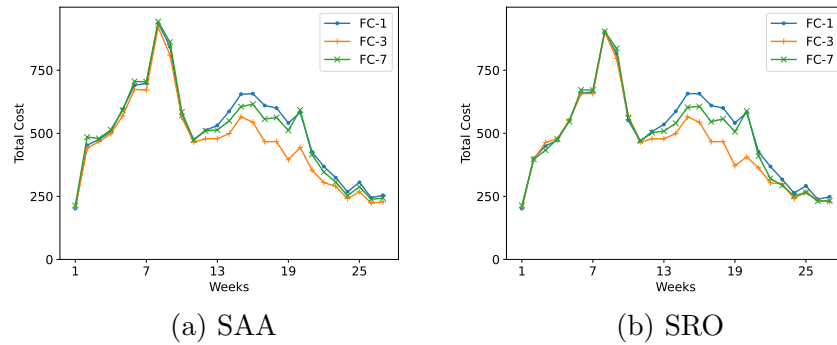


Figure 9 Effect of secondment on the cost as a function of weeks, using base transfer cost 0.1. Here, “FC-1” denotes the one-day secondment scenario, “FC-3” represents the three-day secondment scenario, and “FC-7” represents the seven-day secondment scenario.

costs due to frequent reassignments, while excessively long secondments reduce flexibility and responsiveness in re-deploying nurses to adjust to the changing demand. Additionally, we observe that both the average number of transfers and the total mileage decrease as secondment length increases. This is because longer secondments reduce the frequency of travel—each nurse remains at the assigned hospital longer, thereby spreading travel distances across multiple days rather than requiring daily commutes.

Table 3 Average cost, deployed transfers, and transferred miles per week for SAA and SRO across various secondment scenarios, using base transfer cost 0.1.

Metrics	One-day secondment		Three-day secondment		Seven-day secondment	
	SAA	SRO	SAA	SRO	SAA	SRO
Cost	515.29	501.72	464.13	456.78	506.07	486.77
Deployed transfers	195.66	195.71	140.22	141.27	107.25	127.12
Transferred miles	14131.70	14257.93	9277.61	9553.46	7733.71	7884.81

5.4. Value of Robustness

From Table 2, we observe that the SRO method consistently achieves a lower weekly average cost compared to SAA across different network designs and secondment scenarios. To understand when and under what demand patterns this performance gap becomes most significant, we conduct a more detailed phase-by-phase analysis in this section.

We begin by comparing the weekly costs under the FC network and the baseline secondment scenario. Figure 10a shows the weekly costs for both SRO and SAA, and Figure 10b illustrates the percentage improvement of SRO over SAA. During the early phase of the pandemic—characterized by increasing demand (before Week 10)—SRO shows a 2–6% cost reduction. In contrast, during the

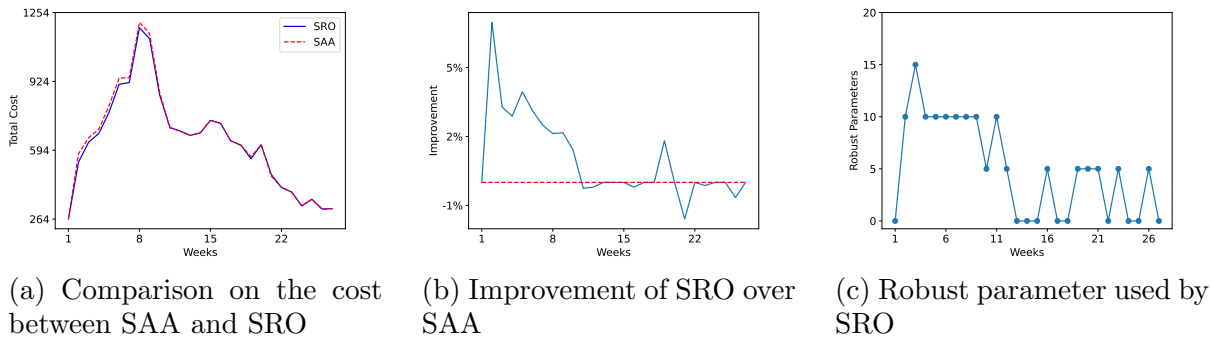


Figure 10 Weekly comparison between SAA and SRO, and robust parameter used by SRO

stable or declining demand phases (Week 10 onward), the performance of SRO and SAA becomes nearly identical (except in weeks 19-20). This latter observation is further supported by the weekly robust parameter selection shown in Figure 10c, where SRO selects a robust parameter value of 0 in most of those weeks after Week 12, effectively reducing to SAA.

To understand the reasons behind these observations, we examine planned nurse transfers from Central, South, and East Hospitals to West Hospital in Figure 11, and from West, East, and South to Central Hospital in Figure 12. We find that, prior to Week 10 (Day 70), SAA consistently under-deploys nurse transfers to high-demand hospitals; whereas SRO tends to allocate more nurses upfront, which reduces the reliance on costly emergency transfers. After Week 10 (Day 71), the planned transfer volumes under SAA become sufficient and align better with demand curve.

To further explore this phenomenon, Figure 13 plots the actual demand, predicted demand (based on rolling three-week historical data), and nurse capacity for a representative sample path. During the increasing demand phase, the rolling forecast lags behind actual trends, leading to systematic underestimation. Since SAA optimizes over the sample average from these forecasts, it under-allocates staff during this phase. In contrast, SRO hedges against this bias by accounting for demand uncertainty in its framework, which leads to better (upfront) deployment and reduced emergency transfers. In the stable or decreasing demand phase, the forecasts tend to align with or overestimate the actual demand (except in outlier weeks such as Weeks 18–19). Consequently, SAA performs well in these periods, and SRO naturally reduces to SAA by selecting a zero robust parameter. In weeks where forecast errors persist, SRO maintains a performance edge. Additional details on forecast accuracy and demand generation are provided in Appendix E.

Sensitivity Analysis. To assess the robustness of our findings, we conduct two sensitivity analyses—one using an alternative demand forecasts and the other using a demand pattern with higher peaks. First, we evaluate a setting where demand predictions are based on six weeks of historical data (instead of three in the baseline). This longer look-back window introduces greater time-lag,

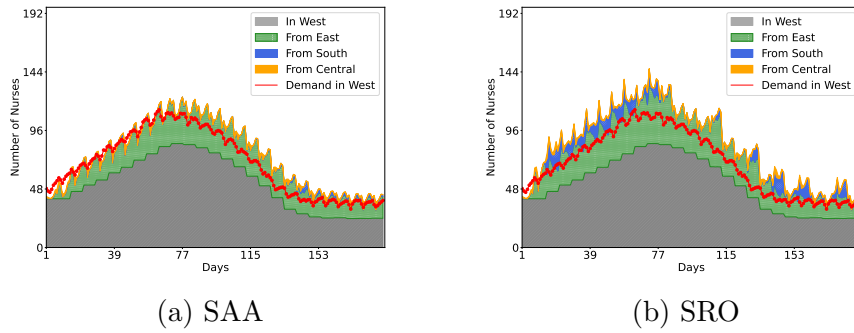


Figure 11 Daily planned nurse transfers to West Hospital for SAA and SRO

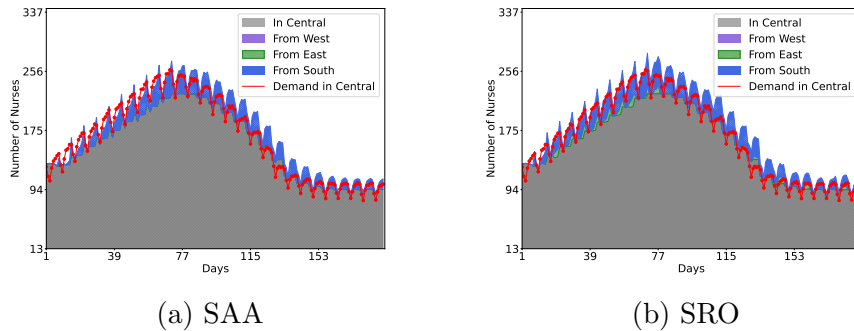


Figure 12 Daily planned nurse transfers to Central Hospital for SAA and SRO

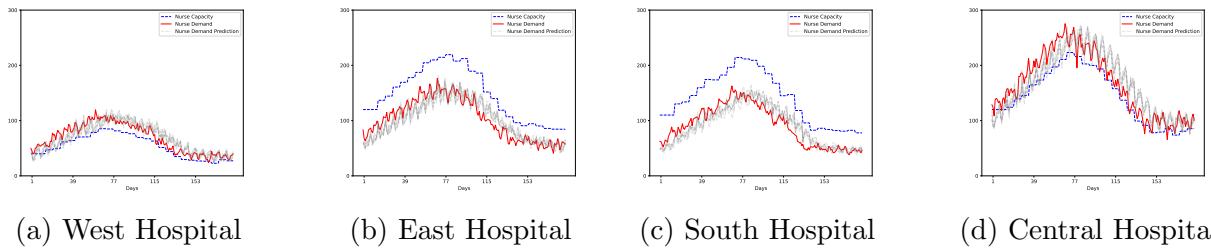


Figure 13 Daily nurse capacity and demand along with the demand prediction (use the data from the past three weeks) at each hospital for one sample path

which exacerbates the underestimation during the increasing demand phase and overestimation during the decline phase. As a result, this amplifies the performance gap between SRO and SAA, for the same reason we explained above. That is, SRO hedges against the forecast bias and proactively transfers more nurses to high-demand hospitals upfront, thereby reducing costly emergency transfers. During stable or decreasing demand phases, both methods behave similarly, and SRO effectively becomes SAA by selecting a robust parameter of zero; see Appendix D.3. Second, we explore an alternative demand scenario by increasing the peak of nurse demand without extending

the time to reach it—simulating a sharper disease spread. We find that SRO shows even greater improvements over SAA during the increasing demand phase. Specifically, SRO allocates more nurses from surplus regions (East and South) to hospitals with shortages (West and Central) early in the planning stage. SAA, in contrast, fails to respond quickly to the sharp rise, resulting in higher shortage costs. See details in Appendix D.4.

5.5. Practical Insights

Our case study reveals several key insights for designing effective nurse redeployment strategies under uncertainty. First, network design emerges as one of the most influential factors: implementing a fully connected network can significantly reduce total transfer costs, volumes, and distances by allowing direct nurse deployments to hospitals facing shortage while avoiding intermediary routing. This effect is more pronounced than variations in secondment length or optimization method, when the secondment length is appropriately calibrated. However, the fully connected design is not universally better—its benefits diminish or even reverse if secondment policies are poorly aligned with network structure, leading to our next insight.

Second, appropriately calibrated secondments are critical. When secondment lengths are appropriately set (particularly longer secondments for rural-to-rural transfers), they can help further reduce total costs and improve nurse well-being by avoiding excessive daily commuting. However, secondment length must be aligned with network structure. If secondments are too short for long-distance deployments (rural-to-rural under fully connected design), high travel costs are incurred, as well as nurse fatigue. Conversely, overly long secondments can limit flexibility and responsiveness to shifting demand, which also degrade system performance. Thus, secondment policy must be carefully aligned with network design to realize the full benefits of connectivity.

Finally, the SRO approach demonstrates better adaptability to demand uncertainty, especially during periods of increasing or underestimated demand. By proactively deploy nurses upfront, SRO reduces costly emergency transfers and improves system responsiveness. In stable or overestimated demand scenarios, SRO converges to SAA, meaning that it maintains efficiency without unnecessary conservatism. Together, these findings highlight the importance of jointly optimizing network design, secondment policy, and robust planning approach to build a cost-effective healthcare workforce system.

6. Conclusions

This paper addresses the challenge of balancing nurse supply and demand across a network of hospitals by developing a strategy for dynamically deploying nurses from overstaffed to understaffed facilities. Given the substantial distances between rural facilities, transferred nurses are provided with advanced notice and are assigned multi-day secondments at the destination hospital to reduce

commute burden, which necessitates a new, multi-stage decision framework that accounts for the temporal correlations caused by the secondments. Moreover, to address uncertainty in demand forecasts, we adopt an SRO approach. We overcome the associated computational challenges of the SRO approach by leveraging linear decision rules and a rolling-horizon framework. Our extensive case study highlights how network design, secondment policies, and optimization methods (SAA vs. SRO) interact to shape system performance. The analysis yields several practical insights: the fully connected network design provides significant benefits under well-calibrated secondment lengths; secondments help reduce both cost and travel burden; and the SRO method shows more value under rising or uncertain demand.

While our framework is designed for hospital-based nurse redeployment, the underlying principles can be applied more broadly to employee transfer programs in other sectors, such as consulting or emergency response. Adapting the model to new domains may require accounting for industry-specific regulations or organizational constraints, but the core methodology remains relevant. An important direction for future work is to integrate individualized nurse staffing into the model, accounting for personal preferences, contractual constraints, and fairness considerations. This extension would enable more tailored and implementable workforce plans, which can further bridge the gap between operational models and real-world staffing needs.

References

- American Hospital Directory (2024) American hospital directory. URL <https://www.ahd.com/>, accessed: 2024-10-02.
- Bélanger V, Ruiz A, Soriano P (2019) Recent optimization models and trends in location, relocation, and dispatching of emergency medical vehicles. *European Journal of Operational Research* 272(1):1–23.
- Benjaafar S, Jiang D, Li X, Li X (2022) Dynamic inventory repositioning in on-demand rental networks. *Management Science* 68(11):7861–7878.
- Bertsimas D, McCord C, Sturt B (2023) Dynamic optimization with side information. *European Journal of Operational Research* 304(2):634–651.
- Bertsimas D, Shtern S, Sturt B (2022) Two-stage sample robust optimization. *Operations Research* 70(1):624–640.
- Bertsimas D, Sim M, Zhang M (2019) Adaptive distributionally robust optimization. *Management Science* 65(2):604–618.
- Brenner A (2025) Combating shortage and burnout with new float pool models. <https://www.inhouse.health/blog-post/combating-shortage-and-burnout-with-new-float-pool-models>, blog post.
- Carayon P, Gurses A (2018) Nursing workload and patient safety—a human factors engineering perspective. *Patient Safety and Quality: An Evidence-Based Handbook for Nurses*, chapter 30 (Rockville, MD:

- Agency for Healthcare Research and Quality (US)), URL <https://www.ncbi.nlm.nih.gov/books/NBK2657/>.
- Chand S, Hsu VN, Sethi S (2002) Forecast, solution, and rolling horizons in operations management problems: A classified bibliography. *Manufacturing & Service Operations Management* 4(1):25–43.
- Cho DD, Bretthauer KM, Cattani KD, Mills AF (2019) Behavior aware service staffing. *Production and Operations Management* 28(5):1285–1304.
- Chou KS, Wong KL, Zhang B, Aguiari D, Im SK, Lam CT, Tse R, Tang SK, Pau G (2023) Taxi demand and fare prediction with hybrid models: Enhancing efficiency and user experience in city transportation. *Applied Sciences* 13(18):10192.
- Cook GN, Goodwin J (2008) Airline networks: A comparison of hub-and-spoke and point-to-point systems. *Journal of Aviation/Aerospace Education & Research* 17(2):1.
- Ding Y, Nagarajan M, Zhang G (2020) Parallel queues with discrete-choice arrival pattern: Empirical evidence and asymptotic characterization. *Available at SSRN 3584880* .
- Glomb L, Liers F, Rösel F (2022) A rolling-horizon approach for multi-period optimization. *European Journal of Operational Research* 300(1):189–206.
- Hao Z, He L, Hu Z, Jiang J (2020) Robust vehicle pre-allocation with uncertain covariates. *Production and Operations Management* 29(4):955–972.
- He L, Hu Z, Zhang M (2020) Robust repositioning for vehicle sharing. *Manufacturing & Service Operations Management* 22(2):241–256.
- Helm JE, Shi P, Drewes M, Cecil J (2024) Delta coverage: The analytics journey to implement a novel nurse deployment program. *INFORMS Journal on Applied Analytics* 54(5):431–454.
- Hoover M, Lucy I, Mahoney K (2024) Data deep dive: A national nursing crisis. URL <https://www.uschamber.com/workforce/nursing-workforce-data-center-a-national-nursing-crisis>, accessed: 2024-05-26.
- Hu Y, Chan CW, Dong J (2025) Prediction-driven surge planning with application to emergency department nurse staffing. *Management Science* 71(3):2079–2126.
- Huh WT, Liu N, Truong VA (2013) Multiresource allocation scheduling in dynamic environments. *Manufacturing & Service Operations Management* 15(2):280–291.
- Indiana State Government (2023) Indiana covid-19 home dashboard. Accessed: 2023-04-22.
- IU Health (2023) Five service regions. Accessed: 2023-04-15.
- Jiang R, Guan Y (2018) Risk-averse two-stage stochastic program with distributional ambiguity. *Operations Research* 66(5):1390–1405.
- Lu M, Chen Z, Shen S (2018) Optimizing the profitability and quality of service in carshare systems under demand uncertainty. *Manufacturing & Service Operations Management* 20(2):162–180.

- Lyons J (2023) Nursing shortage by state: A state-by-state breakdown of the nursing shortage. URL <https://nurse.org/education/nursing-shortage-by-state-analysis/>, accessed: 2024-05-22.
- Meredith P, Turner L, Saville C, Griffiths P (2024) Nurse understaffing associated with adverse outcomes for surgical admissions. *British Journal of Surgery* 111(9):znae215.
- Murphy K (2024) Navigating the u.s. nurse staffing shortage. URL <https://prsglobal.com/blog/navigating-the-us-nurse-staffing-shortage>, accessed: 2025-05-26.
- Nair R, Miller-Hooks E (2011) Fleet management for vehicle sharing operations. *Transportation Science* 45(4):524–540.
- Nelson J (2023) What’s the difference between pcu and icu? Accessed: 2023-04-15.
- Paterson C, Kiesmüller G, Teunter R, Glazebrook K (2011) Inventory models with lateral transshipments: A review. *European Journal of Operational Research* 210(2):125–136.
- Prabhu VG, Taaffe K, Caglayan C, Isik T, Song Y, Hand W (2020) Team based, risk adjusted staffing during a pandemic: An agent based approach. *2020 Winter Simulation Conference (WSC)*, 747–758 (IEEE).
- Raghavan P, Tompson CD (1987) Randomized rounding: a technique for provably good algorithms and algorithmic proofs. *Combinatorica* 7(4):365–374.
- Rath S, Rajaram K, Hudson M, Mahajan A (2023) Multilocation, dynamic staff planning for a healthcare system: Methodology and application. *Dynamic Staff Planning for a Healthcare System: Methodology and Application (August 12, 2023)* .
- Razak F, Shin S, Pogacar F, Jung HY, Pus L, Moser A, Lapointe-Shaw L, Tang T, Kwan JL, Weinerman A, et al. (2020) Modelling resource requirements and physician staffing to provide virtual urgent medical care for residents of long-term care homes: a cross-sectional study. *Canadian Medical Association Open Access Journal* 8(3):E514–E521.
- Ryu M, Jiang R (2025) Nurse staffing under absenteeism: A distributionally robust optimization approach. *Manufacturing & Service Operations Management* .
- Shi P, Helm JE, Chen C, Lim J, Parker RP, Tinsley T, Cecil J (2022) Operations (management) warp speed: Rapid deployment of hospital-focused predictive/prescriptive analytics for the covid-19 pandemic. *Production and Operations Management* .
- Shu J, Chou MC, Liu Q, Teo CP, Wang IL (2013) Models for effective deployment and redistribution of bicycles within public bicycle-sharing systems. *Operations Research* 61(6):1346–1359.
- Song DP, Dong JX (2014) Empty container repositioning. *Handbook of Ocean Container Transport Logistics: Making Global Supply Chains Effective*, 163–208 (Cham: Springer International Publishing).
- Števéřová L, Badánik B (2018) Performance of hub and spoke networks of selected airlines. *Transportation research procedia* 35:240–249.
- University of St Augustine for Health Sciences (2024) Nursing shortage: A 2024 data study reveals key insights. URL <https://www.usa.edu/blog/nursing-shortage/>, accessed: 2025-04-22.

- Wang Y, Nguyen VA, Hanasusanto GA (2024) Wasserstein robust classification with fairness constraints. *Manufacturing & Service Operations Management* 26(4):1567–1585.
- Wolters Kluwer (2016) The importance of the optimal nurse-to-patient ratio. Accessed: 2023-04-16.
- Xie J, Zhuang W, Ang M, Chou MC, Luo L, Yao DD (2021) Analytics for hospital resource planning—two case studies. *Production and Operations Management* 30(6):1863–1885.
- Yankovic N, Green LV (2011) Identifying good nursing levels: A queuing approach. *Operations research* 59(4):942–955.
- Yao X, Shehadeh KS, Padman R (2024) Multi-resource allocation and care sequence assignment in patient management: a stochastic programming approach. *Health Care Management Science* 27(3):352–369.
- Yom-Tov GB, Mandelbaum A (2014) Erlang-r: A time-varying queue with reentrant customers, in support of healthcare staffing. *Manufacturing & Service Operations Management* 16(2):283–299.
- Yuan Y (2025) Managing flexible capacity in service systems with worker shortages. *Manufacturing & Service Operations Management* 27(3):808–824.

Appendix A: Description of Model Notations

Table 4 Description of model notations

Notation	Description
L	Number of hospitals
T	Planning horizon length
ξ_t^i	Nurse demand on day t at location i
$\boldsymbol{\xi}_t = [\xi_t^{ij}, 1 \leq i, j \leq L]$	Demand vector at all locations on day t
$\boldsymbol{\xi}_{[t]} = (\boldsymbol{\xi}_1, \dots, \boldsymbol{\xi}_t)$	Historical nurse demands up to day t
a_t^{ij}	Number of nurses tentatively planned to transfer from location i to location j on day t , where $i, j \in [L]$ and $t \in [T]$
$\mathbf{a}_t = [a_t^{ij}, 1 \leq i, j \leq L]$	Vector of on-call decisions for day t
$\mathbf{a}_{[t]} = (\mathbf{a}_1, \dots, \mathbf{a}_t)$	Sequence of on-call plans from day 1 to day t
b_t^{ij}	Number of nurses deployed from location i to location j on day t
$\mathbf{b}_t = [b_t^{ij}, 1 \leq i, j \leq L]$	Vector of deployment decisions for day t
$\mathbf{b}_{[t]} = (\mathbf{b}_1, \dots, \mathbf{b}_t)$	Sequence of deployment decisions up to day t
ω^{ij}	Minimum required stay from location i to location j when sufficient time remains in the horizon
$\mu^{ij}(t) = \omega^{ij} \wedge (T - t + 1)$	Secondment length for a nurse transferred from location i to location j on day t
p	Daily payment premium for working at a non-home location
τ^{ij}	Additional compensation for traveling from location i to location j
η	Percentage fee for canceling a planned transfer
δ_t^i	Imbalance between demand and available nurses at location i on day t
θ_t	Premium multiplier applied to the daily wage p for emergency transfers on day t
K^i	Initial nurse capacity at location i
$z_t^{ij}(k)$	Number of nurses transferred from location i to location j , having the number of remaining secondment days as k at the beginning of day t (before the actual transfer), $1 \leq k \leq \omega - 1$

Appendix B: Proof

B.1. Proof of Proposition 1

For any sample path $\boldsymbol{\xi}_{[T]}^n$, $1 \leq n \leq N$, the perturbed nurse demand satisfy the following

$$\bar{\zeta}_t^{i,n} = \xi_t^{i,n} - \epsilon_N \leq \zeta_t^i \leq \xi_t^{i,n} + \epsilon_N = \underline{\zeta}_t^{i,n}$$

for $1 \leq t \leq T$ and $1 \leq i \leq L$. We see that the demand perturbations at each location on each day are independent.

Let $x_t^{ij}(\boldsymbol{\zeta}_{[t]}) = (b_t^{ij}(\boldsymbol{\zeta}_{[t]}) - a_t^{ij}(\boldsymbol{\zeta}_{[t]}))^+$ for $1 \leq t \leq T$ and $1 \leq i \leq L$. Then we have

$$(a_t^{ij} - b_t^{ij}(\boldsymbol{\zeta}_{[t]}))^+ = x_t^{ij}(\boldsymbol{\zeta}_{[t]}) - b_t^{ij}(\boldsymbol{\zeta}_{[t]}) + a_t^{ij}. \quad (29)$$

Let $y_t^i(\boldsymbol{\zeta}_{[t]}) = (\delta_t^i(\boldsymbol{\zeta}_{[t]}))^+$ for $1 \leq t \leq T$ and $1 \leq i \leq L$. Then we reformulate Problem (18) as Problem (19).

The two formulations are equivalent since all $y_t^i(\boldsymbol{\zeta}_{[t]})$ can reach their worst case values simultaneously when $\bar{\zeta}_t^{i,n} \leq \zeta_t^i \leq \underline{\zeta}_t^{i,n}$ for $1 \leq t \leq T$ and $1 \leq i \leq L$. Consequently, the summation $\sum_{t=1}^T \sum_{i=1}^L s_t^i y_t^i(\boldsymbol{\zeta}_{[t]})$ achieves its worst-case scenario for the same realization of $\boldsymbol{\zeta}_{[T]}$. The result follows. \square

B.2. Proof of Proposition 2

We transform the worst-case objective of Problem (19) into the following constraints via introducing epigraph variables $v_1, v_2, \dots, v_N \in \mathbb{R}$, following Bertsimas et al. (2023).

$$\sum_{t=1}^T \sum_{i=1}^L \sum_{j=1}^L \left((\theta_t p \mu^{ij}(t) + \tau^{ij}) \left(x_t^{0,ij} + \sum_{m=1}^t \sum_{l=1}^L x_{t,ml}^{1,ij} \zeta_m^l \right) + (\eta - 1)(p \mu^{ij}(t) + \tau^{ij}) \left(\left(x_t^{0,ij} + \sum_{m=1}^t \sum_{l=1}^L x_{t,ml}^{1,ij} \zeta_m^l \right) - \left(b_t^{0,ij} + \sum_{m=1}^t \sum_{l=1}^L b_{t,ml}^{1,ij} \zeta_m^l \right) + a_t^{ij} \right) \right) + \sum_{t=1}^T \sum_{i=1}^L s_t^i \left(y_t^{0,i} + \sum_{m=1}^t \sum_{l=1}^L y_{t,ml}^{1,i} \zeta_m^l \right) \leq v_n, \quad \forall \zeta_{[T]} \in \mathcal{U}_N^n, 1 \leq n \leq N. \quad (30)$$

The constraint can be reformulated as

$$\begin{aligned} & \sum_{t=1}^T \sum_{k=t}^T \sum_{i=1}^L \left(\sum_{j=1}^L \left((\theta_k p \mu^{ij}(k) + \tau^{ij}) \sum_{l=1}^L x_{k,tl}^{1,ij} \zeta_t^l + (\eta - 1)(p \mu^{ij}(k) + \tau^{ij}) \sum_{l=1}^L (x_{k,tl}^{1,ij} - b_{k,tl}^{1,ij}) \zeta_t^l \right) + s_k^i \sum_{l=1}^L y_{k,tl}^{1,i} \zeta_t^l \right) \\ & \leq v_n - \sum_{t=1}^T \sum_{i=1}^L \left(\sum_{j=1}^L \left((\theta_t p \mu^{ij}(t) + \tau^{ij}) x_t^{0,ij} + (\eta - 1)(p \mu^{ij}(t) + \tau^{ij}) (x_t^{0,ij} - b_t^{0,ij} + a_t^{ij}) \right) - s_t^i y_t^{0,i} \right), \\ & \quad \forall \zeta_{[T]} \in \mathcal{U}_N^n, 1 \leq n \leq N. \end{aligned} \quad (31)$$

Similarly, constraint (19c) can be reformulated as

$$\begin{aligned} & \sum_{k=1}^T \sum_{m=k}^T \mathbb{1}_{\{(t-\omega^{ij}+1) \vee 1\} \leq m \leq t} \sum_{j=1}^L \sum_{l=1}^L b_{m,kl}^{1,ij} \zeta_k^l \leq K^i - \sum_{j=1}^L \sum_{k=(t-\omega^{ij}+1) \vee 1}^t b_k^{0,ij}, \\ & \quad 1 \leq i \leq L, 1 \leq t \leq T, \forall \zeta_{[T]} \in \mathcal{U}_N^n, 1 \leq n \leq N, \end{aligned} \quad (32)$$

and constraint (19d) can be reformulated as

$$\begin{aligned} & \sum_{k=1}^T \sum_{m=k}^T \left(\mathbb{1}_{\{(t-\omega^{ij}+1) \vee 1\} \leq m \leq t} \sum_{j=1}^L \sum_{l=1}^L b_{m,kl}^{1,ij} \zeta_k^l - \mathbb{1}_{\{(t-\omega^{ji}+1) \vee 1\} \leq m \leq t} \sum_{j=1}^L \sum_{l=1}^L b_{m,kl}^{1,ji} \zeta_k^l - \mathbb{1}_{\{m=t\}} \sum_{l=1}^L y_{m,kl}^{1,i} \zeta_k^l \right) \\ & \leq y_t^{0,i} + K^i - \sum_{j=1}^L \sum_{k=(t-\omega^{ij}+1) \vee 1}^t b_k^{0,ij} + \sum_{j=1}^L \sum_{k=(t-\omega^{ji}+1) \vee 1}^t b_k^{0,ji} - \zeta_t^i, \quad 1 \leq i \leq L, 1 \leq t \leq T, \forall \zeta_{[T]} \in \mathcal{U}_N^n, 1 \leq n \leq N, \end{aligned} \quad (33)$$

constraint (19e) can be reformulated as

$$\sum_{k=1}^T \sum_{m=k}^T \mathbb{1}_{\{m=t\}} \sum_{l=1}^L (b_{m,kl}^{1,ij} \zeta_m^l - x_{m,kl}^{1,ij} \zeta_m^l) \leq a_t^{ij} + x_t^{0,ij} - b_t^{0,ij}, \quad 1 \leq i, j \leq L, 1 \leq t \leq T, \forall \zeta_{[T]} \in \mathcal{U}_N^n, 1 \leq n \leq N, \quad (34)$$

constraint (19f) can be reformulated as

$$\begin{aligned} & - \sum_{k=1}^T \sum_{m=k}^T \mathbb{1}_{\{m=t\}} \sum_{l=1}^L b_{m,kl}^{1,ij} \zeta_m^l \leq b_t^{0,ij}, \quad 1 \leq i, j \leq L, 1 \leq t \leq T, \forall \zeta_{[T]} \in \mathcal{U}_N^n, 1 \leq n \leq N, \\ & - \sum_{k=1}^T \sum_{m=k}^T \mathbb{1}_{\{m=t\}} \sum_{l=1}^L x_{m,kl}^{1,ij} \zeta_m^l \leq x_t^{0,ij}, \quad 1 \leq i, j \leq L, 1 \leq t \leq T, \forall \zeta_{[T]} \in \mathcal{U}_N^n, 1 \leq n \leq N, \end{aligned} \quad (35)$$

and constraint (19g) can be reformulated as

$$- \sum_{k=1}^T \sum_{m=k}^T \mathbb{1}_{\{m=t\}} \sum_{l=1}^L y_{m,kl}^{1,i} \zeta_k^l \leq y_t^{0,i}, \quad 1 \leq i \leq L, 1 \leq t \leq T, \forall \zeta_{[T]} \in \mathcal{U}_N^n, 1 \leq n \leq N. \quad (36)$$

We see that each semi-infinite constraint can be reformulated as

$$\max_{\zeta_{[T]} \in \mathcal{U}_N^n} \sum_{t=1}^T \beta_t \zeta_t \leq \gamma$$

for some vectors $\beta = (\beta_1, \dots, \beta_T) \in \mathbb{R}^{L \times T}$ and $\gamma \in \mathbb{R}$. It follows from strong duality for linear optimization that

$$\max_{\zeta_{[T]} \in \mathcal{U}_N^n} \sum_{t=1}^T \beta_t \zeta_t = \begin{cases} \min_{\lambda_t, \alpha_t \in \mathbb{R}_+^L} \sum_{t=1}^T (\bar{\zeta}_t^n \lambda_t - \underline{\zeta}_t^n \alpha_t) \\ \text{s.t., } \lambda_t - \alpha_t = \beta_t \quad \forall t \in [T]. \end{cases} \quad (37)$$

The optimal solutions are given by $\lambda_t = [\beta_t]_+$ and $\alpha_t = [-\beta_t]_+$. Importantly, these solutions are independent of the index n of the uncertainty set \mathcal{U}_N^n .

Consequently, constraint (31) is satisfied if and only if there exist $\nu^{epi}, \psi^{epi} \in \mathbb{R}_+^{T \times L}$ such that

$$\begin{aligned} \sum_{t=1}^T \left(\sum_{l=1}^L \nu_{tl}^{epi} \bar{\zeta}_t^{ln} - \sum_{l=1}^L \psi_{tl}^{epi} \underline{\zeta}_t^{ln} \right) + \sum_{t=1}^T \sum_{i=1}^L \left(\sum_{j=1}^L \left((\theta_t p \mu^{ij}(t) + \tau^{ij}) x_t^{0,ij} + (\eta - 1)(p \mu^{ij}(t) + \tau^{ij})(x_t^{0,ij} - b_t^{0,ij} + a_t^{ij}) \right) \right. \\ \left. - s_t^i y_t^{0,i} \right) \leq v_n, \quad 1 \leq n \leq N, \\ \nu_{tl}^{epi} - \psi_{tl}^{epi} = \sum_{k=t}^T \sum_{i=1}^L \left(\sum_{j=1}^L \left((\theta_k p \mu^{ij}(k) + \tau^{ij}) x_{k,tl}^{1,ij} + (\eta - 1)(p \mu^{ij}(k) + \tau^{ij})(x_{k,tl}^{1,ij} - b_{k,tl}^{1,ij}) \right) + s_k^i y_{k,tl}^{1,i} \right), \\ 1 \leq l \leq L, 1 \leq t \leq T. \end{aligned}$$

Constraint (32) is satisfied if and only if there exist $\nu^{cap}, \psi^{cap} \in \mathbb{R}_+^{T^2 \times L^2}$ such that

$$\begin{aligned} \sum_{k=1}^T \left(\sum_{l=1}^L \nu_{klti}^{cap} \bar{\zeta}_k^{ln} - \sum_{l=1}^L \psi_{klti}^{cap} \underline{\zeta}_k^{ln} \right) + \sum_{j=1}^L \sum_{k=(t-\omega^{ij}+1) \vee 1}^t b_k^{0,ij} \leq K^i, \quad 1 \leq i \leq L, 1 \leq t \leq T, 1 \leq n \leq N, \\ \nu_{klti}^{cap} - \psi_{klti}^{cap} = \sum_{m=k}^T \sum_{j=1}^L \mathbb{1}_{\{(t-\omega^{ij}+1) \vee 1 \leq m \leq t\}} b_{m,kl}^{1,ij} \zeta_k^l, \quad 1 \leq i \leq L, 1 \leq t \leq T, 1 \leq l \leq L, 1 \leq k \leq T. \end{aligned}$$

Constraint (33) is satisfied if and only if there exist $\nu^{sho}, \psi^{sho} \in \mathbb{R}_+^{T^2 \times L^2}$ such that

$$\begin{aligned} \sum_{k=1}^T \left(\sum_{l=1}^L \nu_{klti}^{sho} \bar{\zeta}_k^{ln} - \sum_{l=1}^L \psi_{klti}^{sho} \underline{\zeta}_k^{ln} \right) + \zeta_t^i - \left(K^i - \sum_{j=1}^L \sum_{k=(t-\omega^{ij}+1) \vee 1}^t b_k^{0,ij} + \sum_{j=1}^L \sum_{k=(t-\omega^{ji}+1) \vee 1}^t b_k^{0,ji} \right) \leq y_t^{0,i}, \\ 1 \leq i \leq L, 1 \leq t \leq T, 1 \leq n \leq N, \\ \nu_{klti}^{sho} - \psi_{klti}^{sho} = \sum_{m=k}^T \left(\sum_{j=1}^L \mathbb{1}_{\{(t-\omega^{ij}+1) \vee 1 \leq m \leq t\}} \sum_{l=1}^L b_{m,kl}^{1,ij} \zeta_k^l - \sum_{j=1}^L \mathbb{1}_{\{(t-\omega^{ji}+1) \vee 1 \leq m \leq t\}} \sum_{l=1}^L b_{m,kl}^{1,ji} \zeta_k^l - \right. \\ \left. \mathbb{1}_{\{m=t\}} \sum_{l=1}^L y_{m,kl}^{1,i} \zeta_k^l \right), \quad 1 \leq i, l \leq L, 1 \leq t \leq T, 1 \leq k \leq T. \end{aligned}$$

Constraint (34) is satisfied if and only if there exist $\nu^{eme}, \psi^{eme} \in \mathbb{R}_+^{T^2 \times L^3}$ such that

$$\begin{aligned} \sum_{k=1}^T \left(\sum_{l=1}^L \nu_{kltij}^{eme} \bar{\zeta}_k^{ln} - \sum_{l=1}^L \psi_{kltij}^{eme} \underline{\zeta}_k^{ln} \right) + b_t^{0,ij} - a_t^{ij} \leq x_t^{0,ij}, \quad 1 \leq i, j \leq L, 1 \leq t \leq T, 1 \leq n \leq N, \\ \nu_{kltij}^{eme} - \psi_{kltij}^{eme} = \sum_{m=k}^T \mathbb{1}_{\{m=t\}} (b_{m,kl}^{1,ij} \zeta_m^l - x_{m,kl}^{1,ij} \zeta_m^l), \quad 1 \leq i, j, l \leq L, 1 \leq t \leq T, 1 \leq k \leq T. \end{aligned}$$

Constraints (35) and (36) are satisfied if and only if there exist $\nu^{nnb}, \psi^{nnb} \in \mathbb{R}_+^{T^2 \times L^3}$, $\nu^{nny}, \psi^{nny} \in \mathbb{R}_+^{T^2 \times L^2}$ such that

$$\begin{aligned} \sum_{k=1}^T \left(\sum_{l=1}^L \nu_{kltij}^{nnb} \bar{\zeta}_k^{ln} - \sum_{l=1}^L \psi_{kltij}^{nnb} \zeta_k^{ln} \right) &\leq b_t^{0,ij}, \quad 1 \leq i, j \leq L, 1 \leq t \leq T, 1 \leq n \leq N, \\ \nu_{kltij}^{nnb} - \psi_{kltij}^{nnb} &= - \sum_{m=k}^T \mathbb{1}_{\{m=t\}} b_{m,kl}^{1,ij} \zeta_m^l, \quad 1 \leq i, j, l \leq L, 1 \leq t \leq T, 1 \leq k \leq T, \\ \sum_{k=1}^T \left(\sum_{l=1}^L \nu_{kltij}^{nnx} \bar{\zeta}_k^{ln} - \sum_{l=1}^L \psi_{kltij}^{nnx} \zeta_k^{ln} \right) &\leq x_t^{0,ij}, \quad 1 \leq i, j \leq L, 1 \leq t \leq T, 1 \leq n \leq N, \\ \nu_{kltij}^{nnx} - \psi_{kltij}^{nnx} &= - \sum_{m=k}^T \mathbb{1}_{\{m=t\}} x_{m,kl}^{1,ij} \zeta_m^l, \quad 1 \leq i, j, l \leq L, 1 \leq t \leq T, 1 \leq k \leq T, \\ \sum_{k=1}^T \left(\sum_{l=1}^L \nu_{klti}^{nny} \bar{\zeta}_k^{ln} - \sum_{l=1}^L \psi_{klti}^{nny} \zeta_k^{ln} \right) &\leq y_t^{0,i}, \quad 1 \leq i \leq L, 1 \leq t \leq T, 1 \leq n \leq N, \\ \nu_{klti}^{nny} - \psi_{klti}^{nny} &= - \sum_{m=k}^T \mathbb{1}_{\{m=t\}} \sum_{l=1}^L y_{m,kl}^{1,i} \zeta_m^l, \quad 1 \leq i, l \leq L, 1 \leq t \leq T, 1 \leq k \leq T. \end{aligned}$$

Thus, we can remove the epigraph decision variables and the result follows. \square

Appendix C: Additional Details for Simulation Platform

In this section, we describe the simulation platform used in our case study. Section C.1 details the process of calibrating the simulator with COVID-19 data and generating the testing sample paths. Section C.2 presents the procedure for generating training sample paths using rolling demand predictions. Section C.3 explains how we calibrate the transfer cost based on geographical distance between different hospitals. Section C.4 specifies the setup of nurse capacity.

C.1. Simulation Calibration and Testing Path Generation

In this section, we describe the process of calibrating the simulator with COVID-19 data, which is then used to generate the testing sample paths. We first introduce the method for generating patient arrivals at each hospital in Appendix C.1.1. To estimate the patient census at each hospital unit, we introduce the patient flow model within one hospital in Appendix C.1.2, which captures the transition of patients between different units in the hospital. Subsequently, we present the census estimation in Appendix C.1.3. Finally, in Appendix C.1.4 we describe how to use the patient census to generate estimates for nurse demand at each hospital, which are used as the testing sample paths.

C.1.1. Patient Arrivals to Each Hospital We assume that the number of patient arrivals on day t ($t \in [\mathcal{T}]$) at location i ($i \in [L]$) follows a Poisson distribution with an arrival rate of $\lambda_{i,t}$ per day, where $\lambda_{i,t}$'s are temporally correlated across days and spatially correlated across locations. We show the details below; Algorithm 1 provides the corresponding pseudocode.

- **Temporal Correlation:** Inspired by the autoregressive model, we recursively generate the first component of the arrival rate, $\lambda_{i,t}^1$, on day $t \in \{1, 2, \dots, \mathcal{T}\}$ at location $i \in \{1, 2, \dots, L\}$ as

$$\lambda_{i,t}^1 = \beta_{i,t} \sum_{l=1}^p \phi_{i,l} \lambda_{i,t-l}^1 + \zeta_{i,t} \kappa_{i,(t-1)\%Y+1} + \epsilon_t,$$

Algorithm 1 Patient Arrival Generation

- **Input:** $p, Y, t_{\text{lag}}, r, \mathcal{T}, L, \alpha, \beta, \zeta, \gamma, \phi, \theta, \kappa, \epsilon, [\lambda_{i,t}, 1 \leq i \leq L, -p+1 \leq t \leq 0]$
- **Main Iteration:** For each $t \in [\mathcal{T}]$ and $i \in [L]$, perform:
 1. Generate the arrival rate $\lambda_{i,t}$ on day t at location i from

$$\lambda_{i,t} = \lambda_{i,t}^1 + \lambda_{i,t}^2,$$

where

$$\begin{aligned} \lambda_{i,t}^1 &= \beta_{i,t} \sum_{l=1}^p \phi_{i,l} \lambda_{i,t-l}^1 + \zeta_{i,t} \kappa_{i,(t-1)\%Y+1} + \epsilon_t, \quad \epsilon_t \sim N(0, \gamma_{i,t} \kappa_{i,(t-1)\%Y+1}) \\ \lambda_{i,t}^2 &= \sum_{\substack{j=1 \\ j \neq i}}^L \alpha_{ji,t} \theta_{ji} \sum_{l=1+t_{\text{lag}}}^{t_{\text{lag}}+r} \lambda_{j,t-l}^2. \end{aligned}$$

2. Generate the patient arrivals $A_{i,t}$ on day t at location i from

$$A_{i,t} \sim \text{Poisson}(\lambda_{i,t}).$$

- **Output:** $A_{i,t}$
-

where p is the number of days from the past that correlates with patient arrivals on day t , $\phi_{i,l}$ is the temporal correlation factor, $\beta_{i,t}$ is a scaling parameter reflecting the strength of disease spread, $\kappa_{i,(t-1)\%Y+1}$ is the day-of-the-week effect, $\zeta_{i,t} \kappa_{i,(t-1)\%Y+1}$ is the patient arrival by considering the day-of-the-week effect, and $\epsilon_t \sim N(0, \gamma_{i,t} \kappa_{i,(t-1)\%Y+1})$ is a white noise term. We let $\phi = [\phi_{i,t}, 1 \leq i \leq L, 1 \leq t \leq p]$, $\beta = [\beta_{i,t}, 1 \leq i \leq L, 1 \leq t \leq p]$, $\kappa = [\kappa_{i,t}, 1 \leq i \leq L, 1 \leq t \leq Y]$ and $\zeta = [\zeta_{i,t}, 1 \leq i \leq L, 1 \leq t \leq p]$, and $\gamma = [\gamma_{i,t}, 1 \leq i \leq L, 1 \leq t \leq p]$.

• **Spatial Correlation:** To incorporate the spatial factor of the disease spread, we recursively generate the second component of the arrival rate, $\lambda_{i,t}^2$, on day $t \in \{1, 2, \dots, \mathcal{T}\}$ at location $i \in \{1, 2, \dots, L\}$ as

$$\lambda_{i,t}^2 = \sum_{j=1, j \neq i}^L \alpha_{ji,t} \theta_{ji} \sum_{l=1+t_{\text{lag}}}^{t_{\text{lag}}+r} \lambda_{j,t-l}^2,$$

where r is the length of the period during which disease spread from other locations would affect the current location, t_{lag} denotes the delay effects in disease spread, θ_{ij} is the spatial correlation factor between location i and location j , $\alpha_{ij,t}$ is the infectious strength from location i to location j . We let $\theta = [\theta_{ij}, 1 \leq i, j \leq L]$ and $\alpha = [\alpha_{ij,t}, 1 \leq i, j \leq L, 1 \leq t \leq T]$.

With the two components, the arrival rate at location i on day t is calculated as

$$\lambda_{i,t} = \lambda_{i,t}^1 + \lambda_{i,t}^2.$$

For our case study, we set $\mathcal{T} = 189$, $Y = 7$, $p = 7$, $L = 4$. We estimate the parameters of the autoregressive model by fitting it to historical arrival data from an anonymous hospital. The resulting coefficients are

$[\phi_{i,1}, \phi_{i,2}, \dots, \phi_{i,p}] = [0.061, -0.165, -0.042, -0.072, -0.148, 0.035, 0.588]$ for each $i \in [L]$. We set $\alpha_{ij,t}$, $\beta_{i,t}$, $\zeta_{i,t}$, and $\gamma_{i,t}$ as

$$\begin{cases} \alpha_{ij,t} = f_t, \\ \beta_{i,t} = f_t, \\ \zeta_{i,t} = c_i f_t, \\ \gamma_{i,t} = c_i f_t, \end{cases}$$

where

$$f_t = \begin{cases} (c_{peak} - 1) \cdot \sqrt{\frac{t - t_{start}}{t_{peak} - t_{start}}} + 1, & \text{if } t_{start} \leq t < t_{peak}, \\ (c_{peak} - 1) \cdot \sqrt{\frac{t_{end} - t}{t_{end} - t_{peak}}} + 1, & \text{if } t_{peak} \leq t \leq t_{end}, \\ 1, & \text{if } t > t_{end}. \end{cases}$$

Here, we set $t_{start} = 1$, $t_{peak} = 49$, $t_{end} = 119$. We choose $[c_1, c_2, c_3, c_4] = [0.3, 0.4, 0.5, 1]$ to reflect the relative magnitude of patient arrivals at the four hospitals (i.e., West, East, South, and Central) under consideration. We set $c_{peak} = 1.5$ for the experiment discussed in Section 5.1.1 and $c_{peak} = 1.7$ for the experiment discussed in Appendix D.4.

Finally, for θ_{ij} , we have

$$\theta_{ij} = \exp \left(-z \frac{d_{ij}}{\max_{i,j \in \{1, \dots, L\}, i \neq j} d_{ij}} \right),$$

where z is a positive coefficient. Here, we set $z = 6.5$, along with the transition and discharge probabilities to be introduced in Section C.1.2, to ensure that the peak patient census across the four hospitals approximates the total staffed bed capacity of the anonymous hospital network, which operated at full capacity during the height of the pandemic (American Hospital Directory 2024).

Figure 14 displays the historical and simulated arrival rates over 30 weeks for each hospital. The red line denotes the expected arrival rate, while the gray lines show 30 randomly generated realizations. Days -20 to 0 correspond to the three-week historical input that uses in the rolling horizon approach.

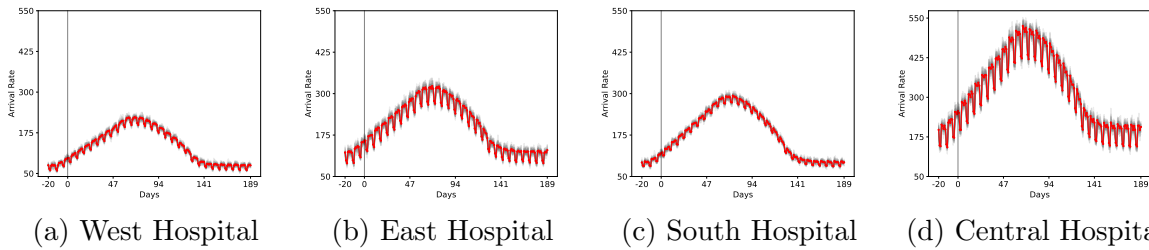


Figure 14 Daily arrival rates for each hospital

C.1.2. Patient Transitions Within the Hospital In this section, we describe the patient transition dynamics across hospital units, which are critical for estimating patient census and, consequently, nurse demand. Each hospital under study contains three unit types: medical-surgical (MS), progressive care (PCU), and intensive care (ICU), differentiated by the level of care required. ICU patients require the most intensive treatment, PCU patients need moderate monitoring, and MS patients typically receive standard inpatient care.

Unit	MS	PCU	ICU	Discharge
MS	0.05	0.2	0.1	0.65
PCU	0.25	0.05	0.1	0.6
ICU	0.5	0.4	0.05	0.05

Table 5 Adjusted probabilities

Unit	MS	PCU	ICU	Discharge
MS	0.7675	0.0125	0.0124	0.2076
PCU	0.0852	0.7463	0.0258	0.1427
ICU	0.1044	0.0596	0.7849	0.0511

Table 6 Estimated probabilities

Figure 15 illustrates the transition behavior of patients among these units. New patients are admitted daily to MS, PCU, or ICU at rates λ_M , λ_P , and λ_I , respectively. We use indices M , P , and I to represent the units. Once admitted to unit $u \in M, P, I$, patients may remain, transfer to another unit, or be discharged (we use index D for discharge), depending on their condition and progression of care needs; see Nelson 2023 for clinical context. The probability of transitioning from unit u to v is denoted by $p_{u,v}$ (if $u = v$, $p_{u,u}$ corresponds to staying in the current unit), and the discharge probability from unit u is $p_{u,D}$ for $u \in M, P, I$. These probabilities satisfy the normalization condition $\sum_{v \in \{M, P, I\}} p_{u,v} + p_{u,D} = 1$.

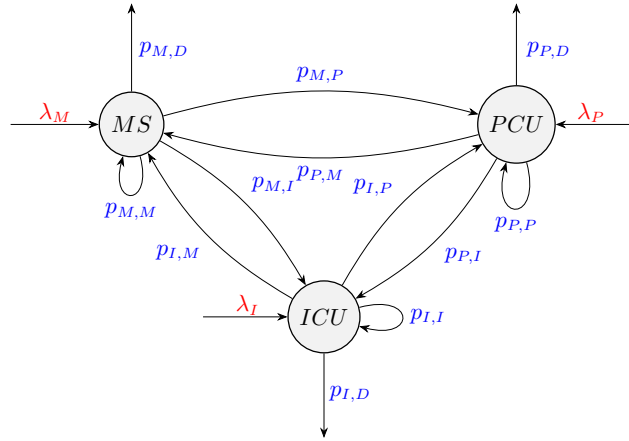


Figure 15 Transition diagram in MS, PCU and ICU

Table 5 presents the set of transition and discharge probabilities used to generate the testing sample paths for each hospital. As noted earlier, these probabilities are calibrated to ensure that the peak patient census aligns with the total staffed bed capacity of the anonymous hospital network. These values are used throughout the numerical study in Section 5. It is important to note that these probabilities differ from those estimated directly from the data. For reference, Table 6 shows the empirically estimated transition probabilities for a representative weekday (Monday). Despite these differences, the managerial insights derived in Section 5 remain robust. For completeness, we provide results using the empirical probabilities in Section E.

C.1.3. Patient Census Estimation Let $N_{i,u}^t$ be the patient census at unit u in hospital i at the beginning of day t . The census on day $t + 1$ can be recursively determined based on the census at day t , accounting for patient inflows (arrivals and transfers-in) and outflows (discharges and transfers-out).

Specifically, we assume that the number of patients staying in the same unit ($n_{i,uu}^t$), are discharged ($n_{i,uD}^t$), or are transferred to other units ($n_{i,uv}^t$ and $n_{i,uw}^t$) in hospital i on day t follows a multinomial distribution,

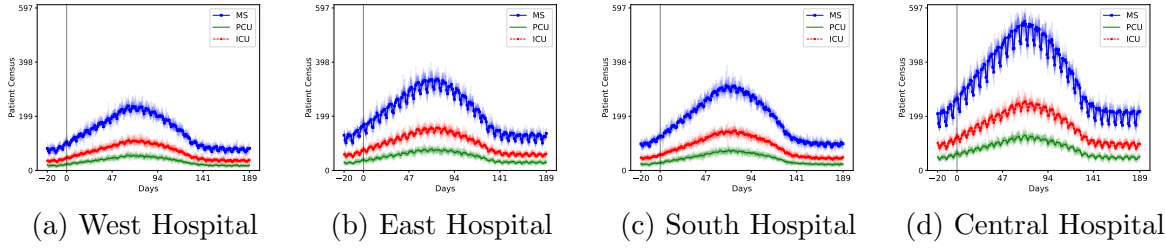


Figure 16 Daily patient census at each unit for each hospital

with parameters $N_{i,u}^t$ and $(p_{i,uu}^{(t-1)\%Y+1}, p_{i,uD}^{(t-1)\%Y+1}, p_{i,uv}^{(t-1)\%Y+1}, p_{i,uw}^{(t-1)\%Y+1})$. Here, $u, v, w \in \{M, P, I\}$ (with $v \neq u$ or $w \neq u$ representing the transfer to a different unit) and the superscript reflects the day-of-week effect. The transition and discharge probabilities are specified in Appendix C.1.2.

For patient arrivals, let $\Lambda_{i,u}^t$ be the number of new patients arriving at unit u in hospital i on day t . We first generate the total number of arrivals, A_i^t , as described in Section C.1.1, and then allocate them across units using a multinomial distribution with parameters A_i^t and probabilities $(q_{i,M}, q_{i,P}, q_{i,I})$, estimated as (0.7659, 0.153, 0.0811) from the anonymous hospital data.

The patient census at each unit at the end of day t is then updated as:

$$N_{i,u}^{t+1} = N_{i,u}^t + \Lambda_{i,u}^t + \sum_{v \in \{M, P, I\}} n_{i,vu}^t - \sum_{v \neq u, v \in \{M, P, I\}} n_{i,uv}^t - n_{i,uD}^t.$$

The corresponding pseudocode is provided in Algorithm 2. Estimated patient censuses for each unit in our case study are shown in Figure 16, with the shaded areas indicating 30 randomly generated trajectories. Days -20 to 0 correspond to the three-week historical input used in the rolling horizon approach.

Algorithm 2 Patient Census Estimation

• **Input:** \mathcal{T} , L , $[A_{i,t}, 1 \leq i \leq L, 1 \leq t \leq \mathcal{T}]$, $[q_{i,u}, 1 \leq i \leq L, u \in \{M, P, I\}]$, $[p_{i,uv}^t, 1 \leq i \leq L, 1 \leq t \leq Y, u, v \in \{M, P, I, D\}]$, $[N_{i,u}^1, 1 \leq i \leq L, u \in \{M, P, I\}]$.

• **Main Iteration:** For each $t \in [\mathcal{T} - 1]$ and $u \in \{M, P, I\}$, perform:

1. Estimate the patient census at unit u in hospital i on day $t + 1$ from

$$N_{i,u}^{t+1} = N_{i,u}^t + \Lambda_{i,u}^t + \sum_{v \in \{M, P, I\}} n_{i,vu}^t - \sum_{v \neq u, v \in \{M, P, I\}} n_{i,uv}^t - n_{i,uD}^t,$$

where

$$(\Lambda_{i,M}^t, \Lambda_{i,P}^t, \Lambda_{i,I}^t) \sim \text{Multinomial}(A_i^t, q_{i,M}, q_{i,P}, q_{i,I}),$$

$$(n_{i,uu}^t, n_{i,uD}^t, n_{i,uv}^t, n_{i,uw}^t) \sim \text{Multinomial}(N_{i,u}^t, p_{i,uu}^{(t-1)\%Y+1}, p_{i,uD}^{(t-1)\%Y+1}, p_{i,uv}^{(t-1)\%Y+1}, p_{i,uw}^{(t-1)\%Y+1}).$$

• **Output:** $N_{i,u}^{t+1}$

C.1.4. Nurse Demand Estimation We adopt the nurse-to-patient staffing ratios used in the anonymous hospital system, which align with standard practices across U.S. hospitals (Yankovic and Green 2011): 1:5 for MS units, 1:3 for PCU, and 1:2 for ICU. Based on these ratios, the nurse demand at hospital i on day t is estimated by aggregating the demand across all units as follows:

$$\xi_i^t = \frac{N_{i,M}^t}{5} + \frac{N_{i,P}^t}{3} + \frac{N_{i,I}^t}{2}.$$

Figure 17 shows the estimated nurse demand for each hospital in our case study. The red line indicates the expected demand, while the gray lines represent 30 randomly generated nurse demand trajectories. Days -20 to 0 correspond to the three-week historical input used in the rolling-horizon forecasting process.

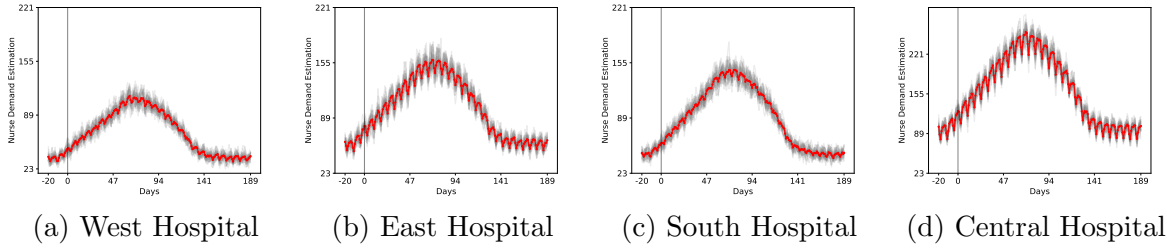


Figure 17 Daily nurse demand estimation for each hospital

C.2. Training Sample Path Generation

In this section, we describe the procedure for generating the training sample paths, which differs from the one used for testing. This distinction is necessary due to the nonstationary nature of patient arrivals and nurse demand, which can lead to significant discrepancies between historical and future patterns. To address this, we adopt a rolling prediction approach: using data from the past three weeks to estimate key patient flow parameters and generate demand forecasts for the upcoming weeks.

Specifically, we estimate the arrival rates, transition probabilities, and discharge probabilities using daily data on patient arrivals, discharges, and inter-unit transfers from the prior three weeks at each hospital. Arrival rates are estimated by taking the day-of-week-specific sample average over three observations (e.g., the past three Mondays), denoted by $\hat{\lambda}_{i,u}^t$ for unit u on day t in hospital i . Transition probabilities— $\hat{p}_{i,uu}^t$, $\hat{p}_{i,uv}^t$, and $\hat{p}_{i,uD}^t$ —are calculated as the average proportion of patients moving between units, also conditioned on the day of the week. Similarly, discharge probabilities $\hat{p}_{i,uD}^t$ are estimated using the same logic. With these estimated parameters, we simulate patient flows and compute nurse demand following the procedures in Sections C.1.3 and C.1.4; the output forms the training sample paths.

C.3. Travel Cost Setting

We set the non-salary transfer cost (i.e., the reimbursement provided to nurses who travel to a remote hospital), denoted by τ_{ij} , based on the geographical distance d_{ij} between hospitals i and j , for all $i, j \in [L]$. The transfer bonuses, distances, and secondment settings across locations were provided in Table 1 in the main paper, and we explain here on how we estimate the values.

To build the connection between the distance and the non-salary bonus, we first establish a baseline by identifying the hospital pair (\hat{i}, \hat{j}) with the shortest distance: $(\hat{i}, \hat{j}) = \arg \min_{i,j} d_{ij}$. We then set the minimum non-salary transfer cost for this pair as $\tau_{\hat{i}, \hat{j}} = \tau_{\hat{j}, \hat{i}} = 1.1$. For all other hospital pairs, we define the non-salary transfer cost as linearly increasing with distance:

$$\tau_{i,j} = \tau_{\hat{i}, \hat{j}} + k(d_{i,j} - d_{\hat{i}, \hat{j}}),$$

where $k = 0.01$ governs the cost increment per unit distance. This linear formulation is consistent with assumptions commonly made in the literature (e.g., Chou et al. 2023).

C.4. Nurse Capacity Setting

We adjust the nurse capacity as outlined in Algorithm 3, using prior nurse capacity levels and historical nurse demand values (ξ 's) to reflect the practice that hospitals adjust staffing levels adaptively based on demand. In our setup, we set $W = 27, L = 4, Y = 7, m = 2$, and $n = 0.8$. The initial nurse capacity for the first two weeks is given by $[C_{1,1}, C_{2,1}, C_{3,1}, C_{4,1}] = [C_{1,2}, C_{2,2}, C_{3,2}, C_{4,2}] = [40, 120, 110, 130]$, and the adjustment scale for each hospital is determined by the hyperparameter vector $[b_1, b_2, b_3, b_4] = [0.11, 0.17, 0.17, 0.115]$. The resulting nurse capacity trajectories for each hospital are illustrated in Figure 18, where the red line indicates the expected capacity and the gray lines represent 30 simulated trajectories.

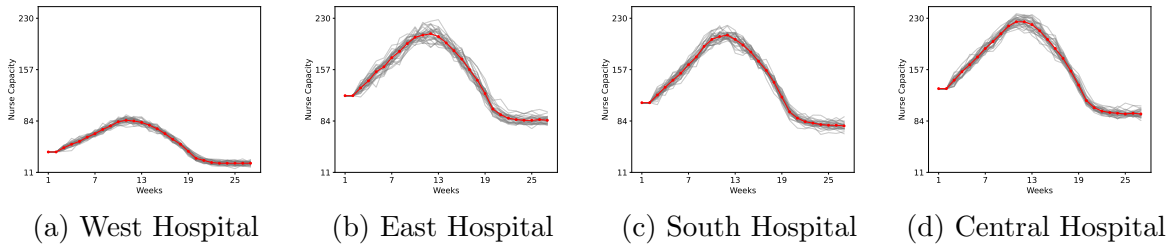


Figure 18 Weekly nurse capacity for each hospital

Appendix D: Supplementary Analysis for Case Study

D.1. Alternative Demand Pattern for Section 5.3

To investigate the effect of secondment beyond the baseline setting, we consider an alternative demand pattern, where only the West Hospital experiences a nurse shortage (the other three hospitals have surplus capacity). The nurse demand and capacity for each hospital are shown in Figure 19. The corresponding results are summarized in Table 7.

D.2. Effect of Coordination Costs on Network Performance

It is important to note that under the FC network, nurses from rural hospitals must be prepared to work in all other rural hospitals, in addition to the Central Hospital. This broader assignment scope may incur a coordination cost – capturing the nurse dissatisfaction stemming from unfamiliarity with multiple workplaces. If we incorporate this cost, the performance of the FC and HS networks then vary depending on the magnitude of this coordination cost. For instance, when the coordination cost is set to 250, the HS network yields a lower

Algorithm 3 Nurse Capacity Estimation

- **Input:** $W, L, Y, m, n, [C_{i,w}, 1 \leq i \leq L], [b_1, \dots, b_L], [\xi_{i,t}, 1 \leq i \leq L, Y(w-3)+1 \leq t \leq WY]$
- **Main Iteration:** For $w \in \{3, 4, \dots, W\}$ and $i \in [L]$, perform:

1. Calculate

$$D_{i,w} = \frac{\sum_{t=Y(w-2)+1}^{Y(w-1)} \xi_{i,t}}{Y} - \frac{\sum_{t=Y(w-3)+1}^{Y(w-2)} \xi_{i,t}}{Y},$$

$$C_{i,w} = C_{i,w-1} + \phi_w(D_{i,w})b_i D_{i,w},$$

where

$$\phi_w(D_{i,w}) = \begin{cases} m, & \text{if } D_{i,w} \geq 0, \\ n, & \text{if } D_{i,w} < 0. \end{cases}$$

- **Output:** $C_{i,w}$
-

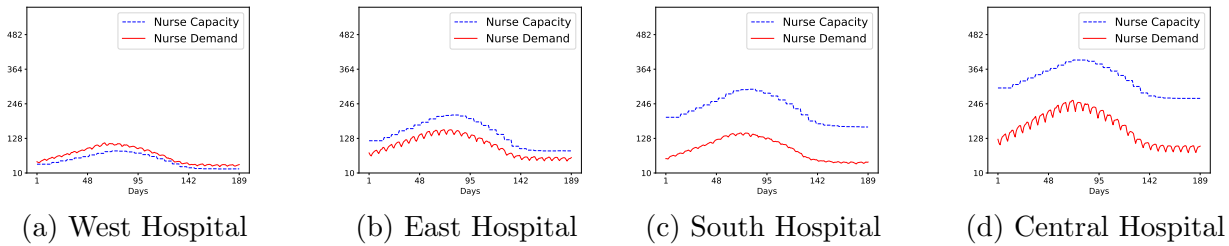


Figure 19 Daily nurse demand and capacity at each hospital under the special demand pattern

Table 7 Average cost, deployed transfers, and transferred miles per week for SAA and SRO across various network designs and secondment scenarios under the alternative demand pattern

Metrics	Network design	Baseline secondment		One-day secondment		Three-day secondment	
		SAA	SRO	SAA	SRO	SAA	SRO
Cost	FC	329.46	325.78	413.50	408.52	302.29	302.29
	HS	358.95	353.25	-	-	-	-
Deployed transfers	FC	67.81	67.83	115.95	116.02	58.43	58.43
	HS	116.08	116.08	-	-	-	-
Transferred miles	FC	7459.06	7461.62	12754.37	12761.94	6427.52	6427.52
	HS	7196.70	7196.70	-	-	-	-

overall cost 933.35 than the FC network (with a cost of 963.30) when the secondment length between rural regions is one, under the SAA approach. However, the FC network outperforms HS when the secondment length is two or more. For example, when the secondment length is two days, the cost is 891.90. A similar phenomenon can be observed under the SRO approach.

D.3. Impact of Time-Lagging in Demand Prediction

In this section, we analyze the case where nurse demand predictions are based on data from the past six weeks (instead of three weeks in the baseline). We show the nurse capacity, and nurse demand along with

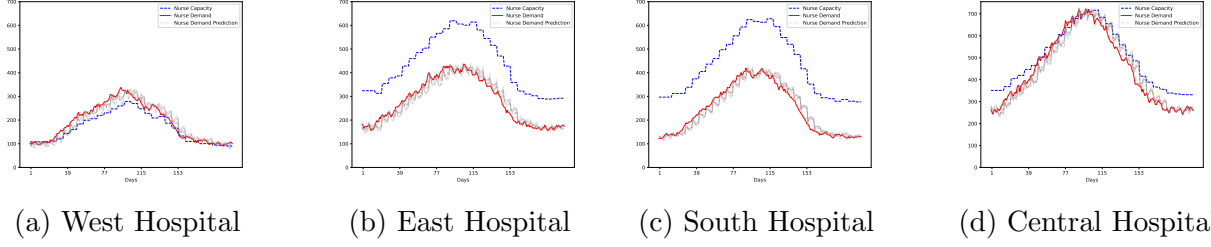


Figure 20 Daily nurse capacity and demand along with the demand prediction (use the data from the past six weeks) for one sample path

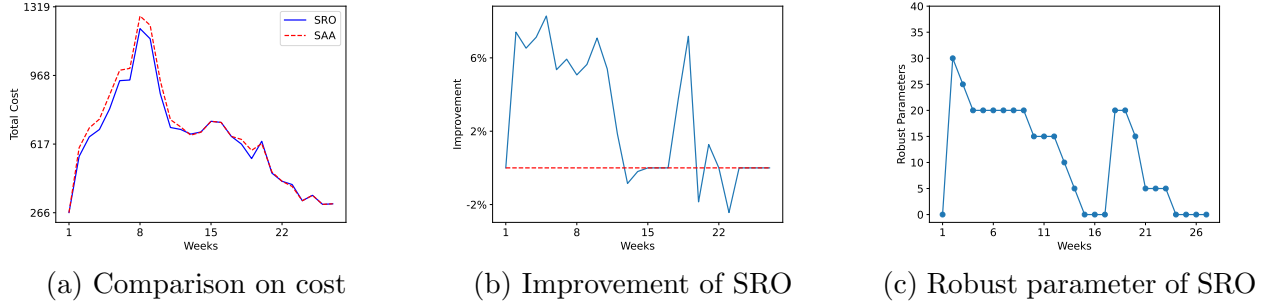


Figure 21 Weekly comparison between SAA and SRO, and robust parameter used by SRO (use the data from the past six weeks)

the nurse demand prediction for a representative sample path in Figure 20. When the demand forecast is based on the past 6-week data, it shows an even greater underestimation of nurse demand during periods of increasing demand, compared to using the three-week data in the baseline. It also shows an even greater overestimation during periods of decreasing demand, due to the time-lagging effect. As a result, we see a even more significant improvements with SRO compared to SAA in Figure 21. In particular, SRO adapts to the potential misestimation of the demand by assigning additional nurses, thereby reducing emergency transfers and achieving superior performance.

D.4. Impact of Higher Demand Peak

In this section, we explore the impact of variations in disease spread on the efficacy of our sample robust optimization approach. Specifically, we modify the disease spread pattern to increase the peak nurse demand while maintaining the same duration to reach this peak, resulting in a sharper increase in demand. The nurse demand and capacity are displayed in Figure 22, and the detailed setting is shown in Appendix C.1. This adjustment enables us to assess how changes in the intensity of demand affect our optimization strategy.

We compare SRO with SAA under the HC network and baseline secondment scenario. Specifically, we analyze the costs associated with SAA and SRO in Figure 23a. We show the improvement of SRO over SAA in Figure 23b, and the chosen robust parameters for SRO in each week are shown in Figure 23c. We see that the improvement of SRO over SAA is greater in the increasing demand phase. This is because West and Central Hospitals experience an even sharper nurse demand and shortage (compared to the baseline), prompting

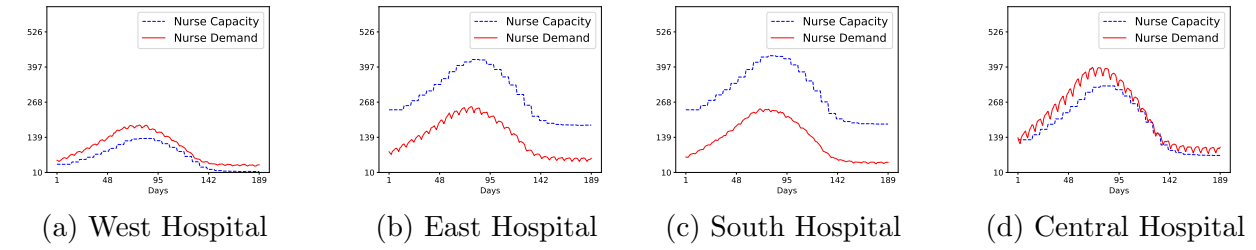


Figure 22 Daily nurse demand and capacity at each hospital (under a higher demand peak)

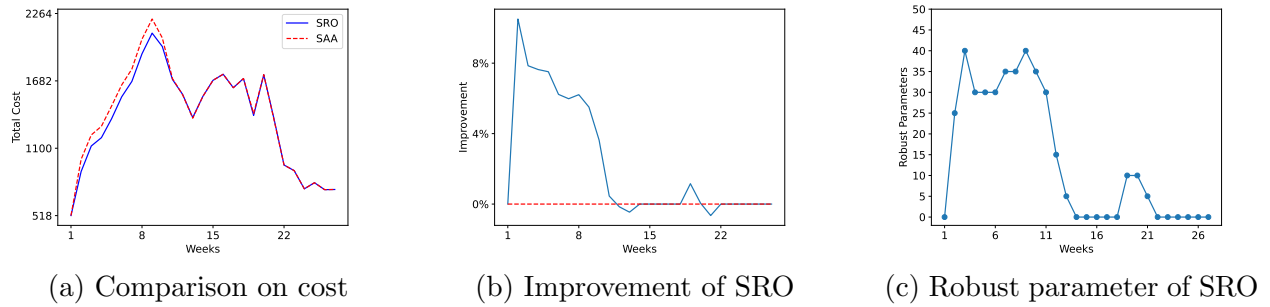


Figure 23 Weekly comparison between SAA and SRO, and robust parameter used by SRO (under a higher demand peak)

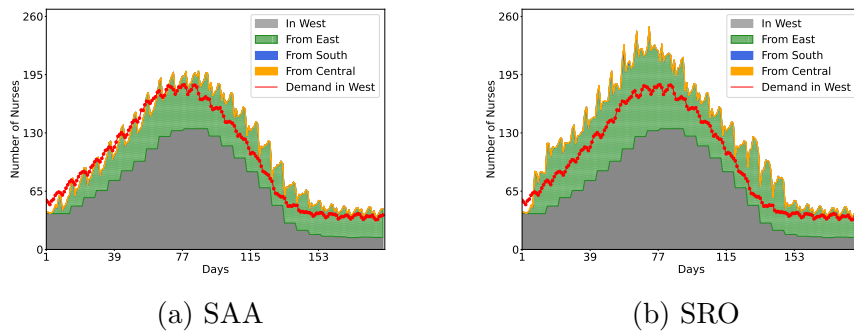


Figure 24 Daily planned nurse transfers to West Hospital for SAA and SRO (under a higher demand peak)

SRO to allocate more nurses from East and South Hospitals to these hospitals during the planning stage, as observed in Figures 24 and 25. That is, SRO is more adaptable to the demand change. In contrast, SAA lacks the flexibility to increase nurse transfers quickly in response to the sudden rise in demand. Consequently, SRO significantly reduces the overall nurse shortage compared to SAA.

Appendix E: Additional Results Using Estimated Transfer Probabilities

In all previous case study experiments, we use the transfer probabilities listed in Table 5. In this section, we show that the managerial insights of the case study in Section 5 still hold when we change to use the probabilities in Table 6. The average nurse demand along with the corresponding nurse capacity under this

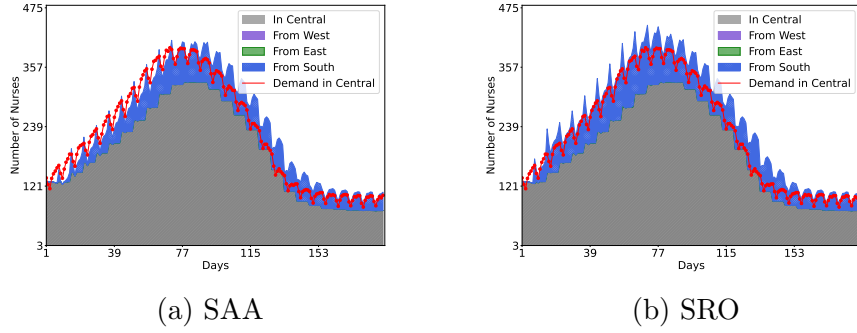


Figure 25 Daily planned nurse transfers to Central Hospital for SAA and SRO (under a higher demand peak)

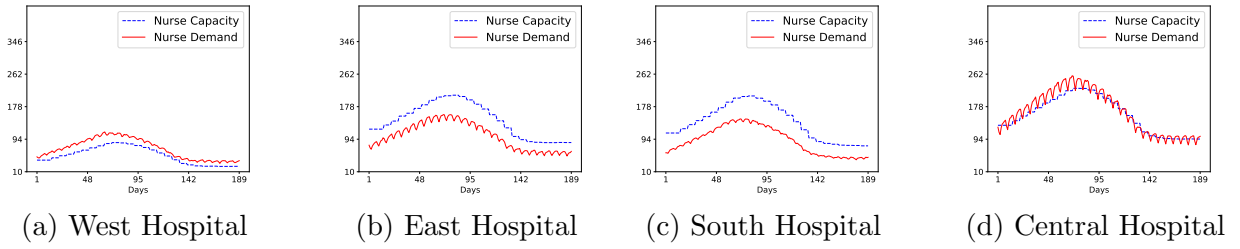


Figure 26 Daily nurse demand and capacity at each hospital using probabilities in Table 6

setting are shown in Figure 26, which have similar patterns as those in Figure 5. We show the effect of network design in Section E.1. Then we examine the effect of secondment in Section E.2. Finally, we show the value of robustness in Section E.3.

E.1. Network Structure

The results under different network design are in Table 8. We see that the total cost under the FC network is much lower than that under the HS network, and the network design has the most significant impact on the total cost compared to the secondment duration and approaches used. This is consistent with the observations in Section 5.2.

Table 8 Average cost per week for SAA and DRO across various network designs and secondment scenarios using probabilities in Table 6

Network design	Baseline secondment		One-day secondment		Three-day secondment	
	SAA	SRO	SAA	SRO	SAA	SRO
FC	1432.8163	1403.16	1658.14	1591.98	1293.89	1282.03
HS	2137.01	2130.38	-	-	-	-

E.2. Effect of Secondment

Next, we examine the effect of secondment length. As shown in Table 8, the total cost decreases with increasing secondment length, as the minimum transfer cost is set to 1.1 in this setting. This makes longer

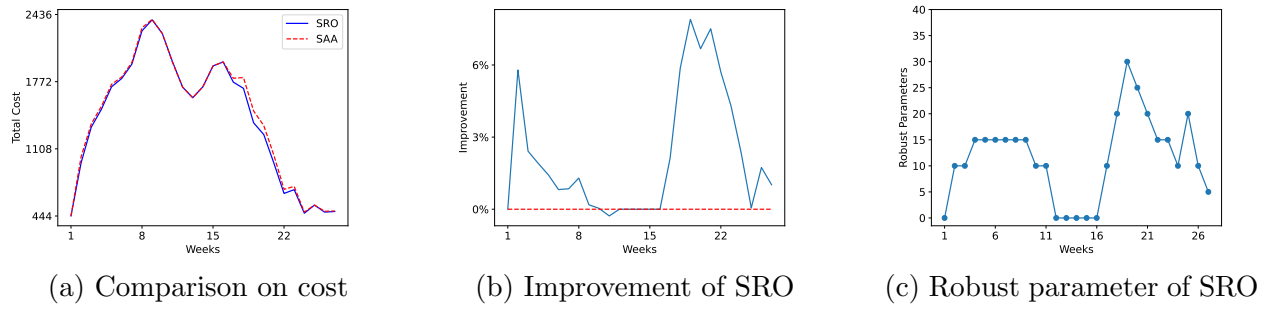


Figure 27 Weekly comparison between SAA and SRO, and robust parameter used by SRO, using probabilities in Table 6

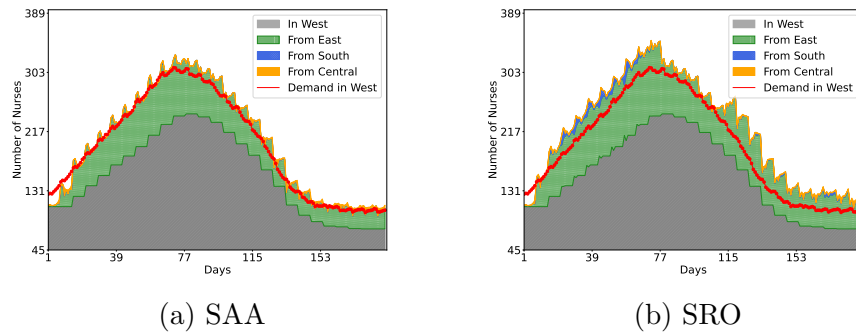
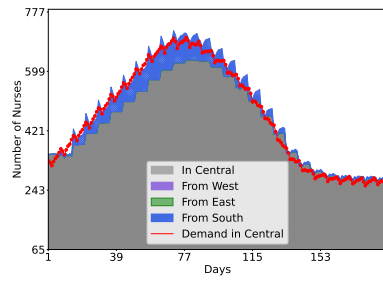


Figure 28 Daily planned nurse transfers to West Hospital for SAA and SRO, using probabilities in Table 6

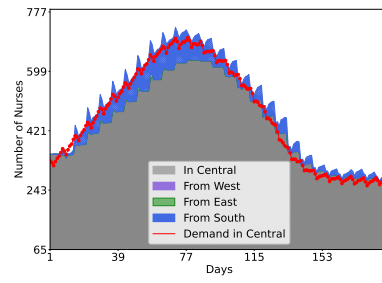
secondments relatively more cost-effective than shorter ones. When we reduce the minimum transfer cost from 1.1 to 0.1, we can observe similar tradeoff from the secondment in Section 5.3.

E.3. Value of Robustness

We present the comparison along with the robust parameter used by SRO in Figure 27. The results indicate that SRO generally outperforms SAA under increasing, decreasing, and stable demand patterns, with only a few exceptions. To understand this difference, we analyze the planned nurse transfers to East and Methodist Hospitals, shown in Figures 28 and 29. We see that SRO assigns more nurses during the planning stage, which helps reduce the need for emergency transfers. In contrast, SAA often fails to assign enough nurses to meet demand. Specifically, SAA generally does not allocate enough nurses during periods of increasing demand and fails to assign adequate staff at the beginning of each week under decreasing and stable demand patterns. This results in a higher number of emergency transfers, which aligns with our findings in Section 5.4.



(a) SAA



(b) SRO

Figure 29 Daily planned nurse transfers to Central Hospital for SAA and SRO, using probabilities in Table 6